Facilitation through Buffer Saturation: Constraints on Endogenous Buffering Properties

V. Matveev[(1)], R. S. Zucker[(2)], and A. Sherman[(3)]

[(1)] Department of Mathematical Sciences and
Center for Applied Mathematics and Statistics
New Jersey Institute of Technology, Newark, NJ 07102

[(2)] Molecular and Cell Biology Department
Neurobiology Division
University of California, Berkeley, CA 94720

[(3)] Laboratory of Biological Modeling, NIDDK
National Institutes of Health
Bethesda, MA 20892

CAMS Report 0304-25, Spring 2004

Center for Applied Mathematics and Statistics

NJIT

April 22, 2004

Facilitation through Buffer Saturation: Constraints on Endogenous Buffering Properties.

Victor Matveev [†], Robert S. Zucker [#], Arthur Sherman [*]

[†] Department of Mathematical Sciences, New Jersey Institute of Technology, Newark, New Jersey 07102

[*] Laboratory of Biological Modeling, National Institute of Diabetes and Digestive and Kidney Diseases, National Institutes of Health, Bethesda, Maryland 20892

[#] Molecular and Cell Biology Department, Neurobiology Division, University of California, Berkeley, California 94720

ABSTRACT

Synaptic facilitation (SF) is a ubiquitous form of short-term plasticity, regulating synaptic dynamics on fast time scales. Although SF is known to depend on the presynaptic accumulation of Ca^{2+}, its precise mechanism is still under debate. Recently it has been shown that at certain central synapses SF results at least in part from the progressive saturation of an endogenous Ca^{2+} buffer (Blatow et al., 2003), as proposed by Klingauf and Neher (1997). Using computational modeling, we study the magnitude of SF that can be achieved by a buffer saturation mechanism (BSM), and explore its dependence on the endogenous buffering properties. We find that a high SF magnitude can be obtained either by a global saturation of a highly mobile buffer in the entire presynaptic terminal, or a local saturation of a completely immobilized buffer. A characteristic feature of BSM in both cases is that SF magnitude depends non-monotonically on the buffer concentration. In agreement with results of Blatow et al. (2003), we find that SF grows with increasing distance from the Ca^{2+} channel cluster, and increases with increasing external Ca^{2+}, $[Ca^{2+}]_{ext}$, for small levels of $[Ca^{2+}]_{ext}$. We compare our modeling results with the experimental properties of SF at the crayfish neuromuscular junction (NMJ), and find that the saturation of an endogenous mobile buffer can explain the observed SF magnitude and its supralinear accumulation time course. However, we show that the BSM predicts slowing of the SF decay rate in the presence of exogenous Ca^{2+} buffers, contrary to experimental observations at the crayfish neuromuscular junction. Further modeling and data are required to resolve this aspect of the BSM.

INTRODUCTION

Short-term synaptic facilitation (SF) is the transient increase of synaptic response that can be elicited by a single action potential (AP) or a short train of APs, and decays on time scales from tens to hundreds of milliseconds. It is observed in a variety of systems, from invertebrate neuromuscular junctions to neocortical synapses (reviewed in Magleby, 1987; Fisher et al., 1997; Zucker, 1994 and 1999; Zucker and Regehr, 2002). The pioneering work of Katz and Miledi (1968) and Rahamimoff (1968) showed that SF depends on the extracellular Ca^{2+}. However, there is still no agreement on the exact nature of the SF mechanism. Arguably, the simplest explanation is that SF results from the accumulation of free residual Ca^{2+} ($[Ca^{2+}]_{res}$) in the presynaptic terminal. This possibility is supported by the extensive evidence that SF is sensitive to manipulations reducing the free intracellular Ca^{2+} (reviewed in Zucker and Regehr, 2002). However, early modeling work (Chad and Eckert, 1984; Simon and Llinás, 1985; Fogelson and Zucker, 1985; Roberts, 1994) demonstrated that the Ca^{2+} concentration in the vicinity of an open Ca^{2+} channel "domain" can reach very high values, from tens to hundreds of μM. This is much higher than the residual $[Ca^{2+}]$ increase caused by a single AP, believed to range from 10 nM to 1 μM (see reviews by Stanley, 1997, Neher, 1998b, Zucker, 1996 and 1999, and Zucker and Regehr, 2002). If the Ca^{2+}-dependent release machinery is located in close proximity to a Ca^{2+} channel, as suggested by the evidence of molecular interactions between the proteins mediating exocytosis and the Ca^{2+} channel proteins (reviewed in Stanley, 1997; Sheng et al., 1998; Catterall, 1999; Fisher and Bourque, 2001; Jarvis and Zamponi, 2001), it is hard to argue that such a small increase in free Ca^{2+} would lead to significant SF. Even taking into account several experimental indications that the Ca^{2+} affinity of the secretory site may be in the 5-20 μM range rather than the 100 μM range (Delaney and Tank, 1994; Ravin et al., 1999; Bollmann and Sakmann, 2000; Schneggenburger and Neher, 2000; Ohnuma et al., 2001), it would not be sufficient to explain the high magnitude of SF observed in many systems. One way to resolve this problem is to assume the presence of a separate high-affinity Ca^{2+}-sensitive site responsible for SF, distinct from the main secretory trigger, and located far enough from a Ca^{2+} channel, where the residual $[Ca^{2+}]$ is comparable to the peak $[Ca^{2+}]$ (Tang et al., 2000). We have recently shown that the properties of SF observed at the crayfish neuromuscular junction (NMJ) can be explained by such a model with two Ca^{2+}-dependent release-controlling sites, given a sufficient separation between the two sites (about 150 nm), and under the additional assumptions of high tortuosity near the active zone and immobilization of Ca^{2+} buffers by the cytoskeleton (Matveev et al., 2002).

An alternative solution is the *bound residual Ca^{2+} hypothesis*, which postulates that SF results from

the build-up of Ca^{2+} bound to the vesicle release sensors (Yamada and Zucker, 1992; Bertram et al, 1996; see also Bennett et al., 1997; Dittman et al., 2000). In fact, this possibility had been suggested in the pioneering studies of Katz and Miledi (1968) and Rahamimoff (1968). Within this framework, the decay time course of SF is determined by the kinetics of Ca^{2+} unbinding from the SF sensor. However, without including the effects of free Ca^{2+} in the model, this possibility is inconsistent with the above-mentioned evidence that SF is sensitive to manipulations of free intracellular Ca^{2+}.

Recently, a third, qualitatively different model of SF was put forward. It was proposed (Klingauf and Neher, 1997; Neher 1998a,b) that the fast presynaptic Ca^{2+} transients elicited by successive depolarizing pulses might themselves increase, as a result of a gradual reduction in the ability of endogenous Ca^{2+} buffers to reduce such transients, due to their progressive saturation (binding) by the residual Ca^{2+} accumulating from pulse to pulse. In this case SF would result from an increase in the size of AP-induced $[Ca^{2+}]$ peaks, rather than an increase in free $[Ca^{2+}]_{res}$, or an increase in the Ca^{2+}-bound state of the release sensor (Table 1). An appealing aspect of the buffer saturation mechanism (BSM) is that it does not assume the presence of a facilitatory Ca^{2+} binding site distinct from the main secretory site, a condition required by the free residual Ca^{2+} model described above. Recently BSM has been shown to play a major role in SF at calbindin-containing neocortical and hippocampal synapses (Blatow et al., 2003), and was also inferred to contribute to SF at the calyx of Held synapse, albeit to a smaller degree (Felmy et al., 2003). The growth of Ca^{2+} transients resulting from buffer saturation has also been observed in Purkinje cells (Maeda et al., 1999) and dentate granule cell axons (Jackson and Redman, 2003). Although the buffer saturation hypothesis has been analyzed in depth by Neher (1998a) using approximate analytic methods (see also Bennett et al., 2000; Trommershäuser et al., 2003), there has yet been no rigorous systematic analysis of the conditions necessary to achieve significant SF within this framework. In the present work we use computer simulations of the presynaptic spatio-temporal Ca^{2+} dynamics to study the properties of the BSM. The numerical approach allows us to consider the widest range of buffering conditions, whereas available analytic techniques rely on approximations that have limited applicability (Neher, 1998a; Pape et al., 1998; Smith et al., 1996; Smith et al., 2001). Our general findings are in agreement with the experimentally observed properties of SF resulting from buffer saturation, as described by Blatow et al. (2003).

Further, we compare our modeling results with experimental recordings at the crayfish NMJ (Tang et al., 2000), to determine whether BSM could underlie the pronounced SF exhibited by this synapse. We find that the saturation of a fast mobile buffer can indeed successfully reproduce the supralinear accumulation time course of SF, as well as the bi-phasic decay time course of SF observed at the crayfish

NMJ. However, BSM predicts a reduction in the SF decay rate by exogenously applied buffers, whereas the opposite effect has been observed experimentally by Tang et al. (2000). We conclude that the involvement of buffer saturation in SF at the crayfish NMJ cannot be established with certainty, until more experimental data is available on Ca^{2+} homeostasis on short time scales in this preparation (see Discussion).

METHODS

Geometry. For simplicity, we represent the presynaptic crayfish motor bouton by a sphere 3 μm in diameter (Fig. 1), which approximates the shape and size of real boutons (Cooper et al., 1995). The surface of the bouton is covered with active zones (AZs), with a density of 1 AZ per 2.56 μm^2 (Cooper et al., 1995; Tang et al., 2000). It is assumed that all AZs are equivalent, and are distributed uniformly over the surface of the spherical bouton. This allows us to restrict our simulations to a conical region 1.8 μm in diameter at its base, surrounding a single AZ, yielding a cone base area close to 2.56 μm^2. We impose reflective boundary conditions for Ca^{2+} and buffer(s) on the sides of the cone, thereby assuming that the Ca^{2+} and buffer fluxes flowing into the cone from the neighboring AZ regions are balanced by the equal fluxes flowing out of the cone. This simplified geometry allows us to perform simulations in rotationally symmetric spherical (r, θ) coordinates, instead of solving the problem in full three dimensions. A similar method has been used by Klingauf and Neher (1997). The reduction from three to two dimensions significantly reduces the computational intensity of the simulations, allowing us to study the behavior of facilitation as two parameters are varied at a time (Figs. 3, 5-6, 8-9, 13). This conical geometry is a rough approximation since the surface of a sphere cannot be tiled with disks, but the inaccuracy introduced by this simplification does not affect the qualitative features of our results.

Ultrastructural reconstruction of the crayfish NMJ has shown that the vesicles are located around the edge of the Ca^{2+} channel cluster (Cooper et al., 1996; Atwood et al., 1997). Therefore, we are interested in the Ca^{2+} concentration achieved at the periphery of the model AZ, at different lateral distances from the edge of the channel cluster, and just below the membrane, as shown in Fig. 1 (*top*). The Ca^{2+} channels belonging to a single AZ are lumped together in our simulations, and the Ca^{2+} current is distributed uniformly over a disk area 160 nm in diameter (Eq. 4; Fig. 1), approximating the size of a channel cluster in a typical AZ (see Fig. 6 *Be, Bf* of Atwood and Karunanithi, 2002). Vesicles themselves are not included in the simulations. The described geometry approximates the rectangular three-dimensional geometry used in the simulations of Tang et al. (2000) and Matveev et al. (2002), with the difference that the individual Ca^{2+} channels are not resolved in the current study. Ignoring the point-like nature of Ca^{2+}

influx is justified since we are not interested in an accurate description of the Ca^{2+} concentration profile in the microdomain of a single channel. As will be shown in Results, sufficient facilitation magnitude is achieved at distances of at least 40-60 nm away from the edge of the cluster, which is larger than the average separation between neighboring Ca^{2+} channels. We expect the effect of the Ca^{2+} influx localization to be small at these distances, as confirmed by comparing our results with modified simulations in which Ca^{2+} influx was localized, with half entering exactly at the center and the rest entering uniformly along the edge of the AZ (i.e., the circumference of the 160 nm disk). We found that the two simulations yielded nearly identical results. Thus, we are interested in what has been previously termed the "submembrane" Ca^{2+} domain (Klingauf and Neher, 1997; Bennett et al., 2000), or an AZ macrodomain. The uniformity assumption for the current distribution may also be viewed as averaging over varying positions of Ca^{2+} channels at individual AZs.

Equations describing buffered diffusion of Ca^{2+}. For simplicity, in most of our simulations we assume the presence of a single dominant Ca^{2+} buffer, with the Ca^{2+} binding reaction described by

$$B + Ca^{2+} \underset{k_{off}}{\overset{k_{on}}{\rightleftharpoons}} CaB \qquad (1)$$

where k_{on} and k_{off} are respectively the binding and the unbinding rates of the Ca^{2+}-buffer compound. This leads to the following reaction-diffusion equations for the Ca^{2+} concentration, $[Ca^{2+}]$, and the concentration of the free (unbound) buffer, [B]:

$$\frac{\partial [Ca^{2+}]}{\partial t} = D_{Ca} \nabla^2 [Ca^{2+}] - k_{on} [Ca^{2+}][B] + k_{off} (B_{total} - [B]) + \frac{1}{2F} I_{Ca}(t)\, g(\theta)\, \delta(r - r_b) \qquad (2)$$

$$\frac{\partial [B]}{\partial t} = D_B \nabla^2 [B] - k_{on} [Ca^{2+}][B] + k_{off} (B_{total} - [B]) \qquad (3)$$

Here D_B and D_{Ca} are the diffusion coefficients in cytosol of the buffer and Ca^{2+}, respectively. We choose D_{Ca}= 0.2 μm^2 ms^{-1} (Allbritton et al., 1992). Following the standard convention, in Eqs. 2 and 3 we have assumed that the initial distribution of the buffer is spatially uniform, and that the diffusion coefficient of the buffer is not affected by the binding of a Ca^{2+} ion. Under these assumptions the sum of the bound and the unbound buffer concentrations is constant in space and time, and is equal to the total buffer concentration, B_{total}. This allows one to eliminate the equation for the evolution of the concentration of the bound buffer, $[CaB] = B_{total} - [B]$. Equations 2-3 are extended in a straightforward way when

simulations include more than one buffer. In this case, each of the buffers evolves according to an equation identical to Eq. 3, and Eq. 2 is expanded to include the binding and the unbinding terms for each of the buffers present (e.g., see Smith et al., 2001).

The last term in Eq. 2 represents the Ca^{2+} influx, where F is Faraday's constant, $I_{Ca}(t)$ is the (inward) calcium current per active zone, and $\delta(r - r_b)$ is the Dirac delta function, with r_b=1.5 μm equal to the bouton radius (this describes a Ca^{2+} current flowing through the surface membrane). The surface density function $g(\theta)$ determines the distribution of the Ca^{2+} current over the AZ surface; it is assumed to be uniform across a disk surface area 160 nm in diameter (S_{Ca}), and is zero everywhere else, as illustrated in Fig. 1 (see justification above). The integral of $g(\theta)$ over the S_{Ca} area should be equal to one, from which we obtain

$$g(\theta) = 1 / S_{Ca} = 1 / (2 \pi r_b^2 (1 - \cos \alpha)) \sim 1 / (\pi r_b^2 \alpha^2) \quad \text{for } \theta \le \alpha \tag{4}$$

$$g(\theta) = 0 \quad \text{for } \theta > \alpha$$

where α is the angle corresponding to the edge of the Ca^{2+} influx area: α = 80 nm / r_b = 0.0533 rad. $I_{Ca}(t)$ is represented as a train of simple 1 ms-long constant current pulses. Unless otherwise noted, we set I_{Ca} magnitude to 11.7 pA. This value is a factor of 2 greater than the estimate of I_{Ca}=5.85 pA obtained by measuring residual [Ca^{2+}] per AP (Yamada and Zucker, 1992; Tang et al., 2000), and is within the range of I_{Ca}=10-50 pA inferred from the measurements of [Ca^{2+}] rise rate during sustained stimulation (Tank et al., 1995; both values are translated to a 1 ms-long current pulse). In Results, we discuss the behavior of the model for variable magnitude of I_{Ca}.

Reflective boundary conditions hold for both [Ca^{2+}] and [B] at all boundaries, except for the boundary condition for [Ca^{2+}] on the top surface of the cone, which assumes Ca^{2+} extrusion by surface pumps:

$$\frac{\partial [Ca^{2+}]}{\partial r} + \frac{M}{D_{Ca}} \frac{[Ca^{2+}]}{[Ca^{2+}] + K_P} = 0 \tag{5}$$

Here M is the maximal pump rate, and K_P is the pump dissociation constant. We use values of K_P=0.2 μM (Dipolo and Beauge, 1983; Carafoli, 1987) and M=0.01 μM μm ms^{-1} (except for Fig. 12 *A, B*). At low [Ca^{2+}], this yields a Ca^{2+} clearance time constant of $\tau \sim (1 + \kappa_0) V K_P / (M S) = 5$ sec, where V and S are the volume and the surface area of the bouton (Fig. 1), and κ_0=500 is the resting state endogenous buffering capacity at the crayfish NMJ (Tank et al., 1995). This agrees with the experimental value of

Ca^{2+} clearance rate obtained by Tank et al. (1995). In Results, we will discuss the possibility of higher Ca^{2+} extrusion rates. The resting buffering capacity κ_0 (also known as the endogenous *buffering ratio* or the *binding ratio*) is an important characteristic of the buffering strength, defined as (Irving et al., 1990; Neher and Augustine, 1992)

$$\kappa_0 \equiv \left.\frac{\partial[\mathrm{CaB}]}{\partial[\mathrm{Ca}^{2+}]}\right|_{\mathrm{rest}} = \frac{\mathrm{B}_{\mathrm{rest}}}{\mathrm{K}_\mathrm{D} + \mathrm{Ca}_{\mathrm{rest}}} = \frac{\mathrm{B}_{\mathrm{total}}\,\mathrm{K}_\mathrm{D}}{(\mathrm{K}_\mathrm{D} + \mathrm{Ca}_{\mathrm{rest}})^2} \tag{6}$$

The relevant free parameters in the model are summarized in Table 2. Instead of the pair of values of k_{off} and k_{on}, we will use either k_{on} and K_D (where $K_D = k_{off} / k_{on}$ is the dissociation constant) or k_{off} and K_D as the two independent parameters describing the buffer-Ca^{2+} interaction. Note that for a fixed K_D, kinetic rates k_{on} and k_{off} are proportional to each other, so in the fixed K_D case the value of k_{on} (k_{off}) characterizes the buffer-Ca^{2+} equilibration kinetics, not just the binding (unbinding) rate. The upper bound of 1 $\mu M^{-1} ms^{-1}$ imposed on the magnitude of k_{on} is close to the theoretical diffusion limit on the maximal achievable forward binding rate for reactants with diffusion coefficients of 0.2 $\mu m^2\ ms^{-1}$ (Keizer, 1987).
To further simplify the analysis, we assume that the resting Ca^{2+} concentration, Ca_{rest}, is zero. In this case the expression for the buffering capacity (Eq. 6) reduces to $\kappa_0 = B_{total}/K_D$. However, all our results can be straightforwardly translated to the case of non-zero Ca_{rest}, as described in the Appendix. In effect, we subtract out Ca_{rest} from the total Ca^{2+} concentration and subtract the initial bound buffer concentration from B_{total}, since these are constant background values that do not affect the dynamics of Ca^{2+} diffusion. Therefore, everywhere in this paper the value of B_{total} should be understood as the initial (resting) total concentration of *free* buffer, B_{rest}.

Numerical simulations. The reaction-diffusion equations 2-33 were solved using the *CalC* ("Calcium Calculator") software developed by one of us (V.M.). *CalC* uses an Alternating-Direction Implicit finite-difference method, second order accurate in spatial and temporal resolution (Morton and Mayers, 1994). To preserve the accuracy of the method in the presence of the buffering term, the equations for [Ca^{2+}] and [B] are solved on separate time grids, shifted with respect to each other by half a time step (Hines, 1984). *CalC* uses an adaptive time-step method; the spatial grid size is adjusted to limit the error tolerance to at most 1-2 % (grid of 36 x 36 points in the mobile buffer case, and 70 x 70 in the fixed buffer case). *CalC* is freely available from *http://web.njit.edu/~matveev*, and runs on Linux, SGI and Windows/Intel platforms.

To ensure reproducibility of this work, the commented simulation script files generating the data reported here will be made available on the above web site.

RESULTS

Facilitation of Ca^{2+} transients: an example.

Figure 2 simulates the buffer saturation mechanism of SF, showing the facilitation of Ca^{2+} transients (FCT) in response to a train of five equal Ca^{2+} current steps. This growth in simulated peak $[Ca^{2+}]$ transients is caused by the residual Ca^{2+} accumulating from pulse to pulse and gradually binding and depleting the free buffer, thereby reducing more and more the ability of the buffer to shunt the AP-triggered Ca^{2+} transients. Note that the *free* $[Ca^{2+}]_{res}$ is negligibly low (see the inset), since most of the residual Ca^{2+} is in fact bound to the buffer, due to a high buffering ratio in our example ($\kappa_0=B_{total}/K_D=1000$). In this and most of the following figures, concentration is shown at a distance of 60 nm from the edge of the Ca^{2+} influx region (site *2* in Fig. 1); dependence on distance will be analyzed later on (see Fig. 6).

The buffer included in the simulation is very mobile, with the diffusion coefficient of D_B=0.2 μm^2 ms^{-1}, which is close to the putative mobility of ATP, for example (Naraghi and Neher, 1997). As will be shown below, strong mobility is a crucial requirement for the BSM. Because of high mobility and fast binding, the Ca^{2+} and the buffer are in equilibrium with each other and evenly distributed in space by the end of each 10 ms-long interpulse interval (data not shown). Therefore, the increase in the fifth Ca^{2+} transient, P_5, over the first Ca^{2+} transient, P_1, is completely determined by the reduction in the amount of free buffer remaining before the last pulse, denoted ΔB ($\Delta B = B_{total} - B_R$). Even at moderate values of the buffering capacity (κ_0>10), almost all of the incoming Ca^{2+} becomes buffer-bound, so that ΔB is approximately equal to the total (volume-averaged) Ca^{2+} influx, and therefore is solely determined by the magnitude of I_{Ca}.

The conditions for high FCT

We will quantify FCT by the ratio of the amplitudes of the fifth and the first peaks in Ca^{2+} concentration:

$$FCT = P_5 / P_1 = 1 + \Delta P / P_1. \quad (7)$$

To achieve significant FCT, one needs a large increase in the Ca^{2+} transient magnitude (ΔP), and a comparatively small value of the first Ca^{2+} transient, P_1 (see Fig. 2). These two requirements lead to two different sets of constraints on model parameters:

1. The requirements for small P_1 are straightforward and include all conditions that increase the buffering efficiency: (i) large B_{total}; (ii) fast binding (large k_{on}); (iii) high buffer mobility, D_B; (iv) small I_{Ca}.

2. The conditions for large ΔP are two-fold: (i) significant buffer saturation/depletion ΔB should be achieved *before* the fifth pulse; as discussed above, this requires moderately high values of κ_0 ($\kappa_0 > 10$), and high I_{Ca}; (ii) for this reduced buffer availability to make a difference, the buffer should be close to saturation *during* the last pulse, as well: the free buffer remaining at the end of the last pulse, B_P, should be small. In other words, initially the buffer should be effective in limiting the rise in Ca^{2+}, but at the end of the train, Ca^{2+} transients should be able to strongly saturate the buffer. This condition is easier to satisfy for low B_{total}, low mobility, D_B, and fast Ca^{2+}-buffer binding (high k_{on}).

Notice that some requirements in the two groups coincide (large k_{on}), whereas the conditions on D_B, B_{total} and I_{Ca} are in contradiction. Therefore, one may expect the FCT to grow monotonically with increasing k_{on}, but its behavior with respect to D_B, B_{total} and I_{Ca} may be non-monotonic. The results presented below confirm this conclusion.

FCT peaks at a finite value of B_{total}, and grows monotonically with increasing k_{on}.

Figure 3 shows the dependence of the five-pulse FCT, defined according to Eq. 7, as a function of K_D and B_{total}, the first two model parameters in Table 2. In this figure the magnitude of the unbinding rate k_{off} is kept fixed (k_{off} =0.4 ms^{-1} for panel *A*, k_{off} =0.1 ms^{-1} for panel *B*), so the value of k_{on} varies along with the value of K_D, according to the relation $k_{on} = k_{off} / K_D$. The similarity between FCT values in Figs. 3 *A* and 3 *B* demonstrates that FCT is only weakly dependent on k_{off}, and is predominantly determined by the values of k_{on} and B_{total} (note that the range of values of k_{on}, indicated along the right margin, are equivalent in the two panels). However, the lower the value of k_{off}, the lower should be K_D to achieve a given FCT magnitude.

In agreement with the conditions formulated in the previous subsection, Fig. 3 shows that FCT grows monotonically with increasing k_{on}, but depends non-monotonically on the value of B_{total}. For any given

value of k_{on} (K_D), maximal FCT is achieved at a certain finite value of B_{total}, which we will denote by B^*_{total} (gray curve in Fig. 3). Explaining this behavior, Figure 4 shows the Ca^{2+} and buffer concentration time courses for three values of B_{total} that correspond to '+' labels in Fig. 3 *A*. The middle '+' marks the optimal value of B^*_{total} (450 μM) for K_D=0.5 μM (Fig. 4 *B*), corresponding to the maximal FCT magnitude, whereas the two flanking values of B_{total} yield smaller values of facilitation. For $B_{total} < B^*_{total}$ (Fig. 4 *A*, B_{total}=200 μM), the buffer is completely saturated during the Ca^{2+} current pulses; even though ΔP is very large in this case, the first Ca^{2+} transient is large as well, resulting in smaller FCT compared to its value for the optimal $B_{total}=B^*_{total}$. In contrast, when $B_{total} > B^*_{total}$ (Fig. 4 *C*, B_{total} =1 mM), the buffer does not saturate to a sufficient extent, so even though the value of P_1 is much reduced compared to Figs. 4 *A* and *B*, the magnitude of ΔP is quite small, leading again to a smaller value of FCT than in the optimal ($B_{total}=B^*_{total}$) case.

As the above analysis suggests, the optimal buffer concentration B^*_{total} should depend on the number of pulses in the stimulation train. One should expect B^*_{total} to increase with increasing train length, since more buffer is required to produce the same saturation effect for a greater total calcium influx, which is proportional to the number of pulses. Our simulations confirm this conclusion, and show a decrease in B^*_{total} of about 10% when the number of pulses is decreased from five to three (data not shown).

FCT for a fixed value of buffering ratio.

Even though the values of most of the model parameters summarized in Table 2 are not readily available from experiment, the rest-state endogenous buffering capacity, κ_0 (see Eq. 6), can be estimated experimentally using fluorescent dye techniques (Neher and Augustine, 1992). For zero Ca_{rest}, κ_0 is given simply by the ratio B_{total} / K_D. We have chosen a value of 500, used in Tang et al. (2000) and Matveev et al. (2002), and close to the estimate of 600 inferred using the fluorescent Ca^{2+} sensitive dye experiments at the crayfish NMJ by Tank et al. (1995). In Fig. 3, the set of points corresponding to κ_0=500 lie along the diagonal lines.

Constraining the value of κ_0 allows us to eliminate one of the parameters from the pair $\{K_D, B_{total}\}$. That is, having restricted ourselves to a constant value of κ_0 (the diagonal in Fig. 3), in Fig. 5 we can explore the dependence of FCT on an independent variation of k_{on} and B_{total} (the latter now also

determines K_D, since $B_{total}=\kappa_0 K_D$). In the new parameter space of Fig. 5, the locus of points corresponding to any given value of k_{off} is a hyperbolic curve. As an example, Fig. 5 *A* shows the two curves of points that correspond to k_{off} =0.4 ms^{-1} and k_{off} =0.1 ms^{-1}. These two hyperbolae are the images of the fixed-κ_0 diagonal lines in Figs. 3 *A* and 3 *B*, respectively. Thus, Fig. 5 *A* compresses all the fixed-κ_0 information contained in a whole family of figures like Figs. 3 *A* and 3 *B*. Moving vertically from one hyperbolic curve to the other in Fig. 5, we see that faster buffers would give greater FCT. Finally, the FCT peak in Fig. 5 *A* shows that the maximal magnitude of FCT is still achieved at a certain finite value of B_{total} (= 500 K_D), even under the fixed κ_0 constraint.

Interestingly, we find that the dependence of FCT on k_{on} and B_{total} is qualitatively as well as quantitatively similar at different values of κ_0. This follows from our earlier result that FCT is primarily determined by the values of B_{total} and k_{on} (Fig. 3). From the relationship $\kappa_0 = B_{total} / K_D = (B_{total}\, k_{on}) / k_{off}$ it is clear that increasing k_{off}, which leaves FCT almost unchanged (Fig. 3), is equivalent to a decrease in κ_0. Therefore, lowering the value of κ_0, say to κ_0=50 (a 10-fold change), and simultaneously increasing k_{off} 10-fold (10-fold decrease in K_D), results only in a moderate reduction of the FCT magnitude (cf. Figs. 5 *A* and 5 B).

Dependence on I_{Ca} is redundant

Apart from the value of κ_0, the value of I_{Ca} per action potential per AZ can also be estimated using fluorescent Ca^{2+} indicator dye measurements. However, the accuracy of the Ca^{2+} influx measurements is not high, since it depends on the optical calibration of the fluorescent Ca^{2+}-sensitive dye used in the measurements, on the estimates of its concentration, and on the independent estimate of the endogenous buffering capacity, κ_0. Further, one may expect significant variability in I_{Ca} between different AZs, as well as between different NMJ boutons. Therefore, it is important to consider how the variation in the value of I_{Ca} would affect FCT.

As it turns out, the dependence of FCT on the magnitude of Ca^{2+} influx per AP is redundant, since knowing the dependence of FCT on K_D and B_{total}, for a given value of k_{off} (Figs. 3, 5), gives full information about its behavior with respect to I_{Ca}. This is a consequence of the freedom in choosing the units of concentration. The FCT magnitude should not be affected if the three parameters with units of concentration, K_D, B_{total}, and I_{Ca} (current equals concentration times volume per unit time), are rescaled

by the same factor. Thus, if the FCT magnitude is calculated for a given value of the Ca^{2+} current, I_{Ca}, then at any other value of the Ca^{2+} current, $\tilde{I}_{Ca}$, it is given by

$$\mathrm{FCT}(\tilde{I}_{Ca}, B_{total}, K_D; k_{off}) = \mathrm{FCT}(I_{Ca}, aB_{total}, aK_D; k_{off}) \quad (8)$$

where $a \equiv I_{Ca}/\tilde{I}_{Ca}$. It follows then that changing the value of the Ca^{2+} current is equivalent to sliding along the line of constant B_{total} / K_D ratio (Figs. 3, 5).

We have to emphasize that the above redundancy condition only holds for the FCT, and not the facilitation of neurotransmitter release. To obtain an expression similar to Eq. 8 for SF proper, given a particular choice of a Ca^{2+}-dependent exocytosis scheme, the affinity of the release mechanism to Ca^{2+} would have to be scaled along with I_{Ca}, K_D and B_{total} (i.e., it would have to be included in the list of arguments that are multiplied by factor a on the right-hand side of Eq. 8). However, we assume a simple power-law relationship between release and $[Ca^{2+}]$, thus avoiding this complication (see next subsection). A similar caveat concerns the case of non-zero resting free $[Ca^{2+}]$ value, Ca_{rest}: in general, Ca_{rest} would have to be included in the argument list on the left- and right-hand sides of Eq. 8. However, the procedure of subtracting out the Ca_{rest} value, described in Appendix, preserves the scaling freedom expressed by Eq. 8 in the case of non-zero values of Ca_{rest} (the arguments in Eq. 8 are to be understood as the "primed" zero-Ca_{rest} values: see Appendix). Finally, we note that the Ca^{2+} pump dissociation constant K_P (Eq. 5) constitutes yet another concentration parameter, however it mostly affects the decay time course of SF (to be discussed below), and has only moderate influence on the FCT magnitude for short-duration stimulation trains considered here.

Relationship between FCT and facilitation of release.

To compare our simulation results with the magnitude of SF available from experiment, we have to convert the FCT values into a measure characterizing facilitation of neurotransmitter release. We prefer not to constrain ourselves to a particular choice of a Ca^{2+}-dependent release model, since doing so would require introduction of additional parameters into our problem. Instead, we will assume that the synaptic response is given by the fourth power of $[Ca^{2+}]$. Then, SF is likewise given by the fourth power of FCT:

$$\mathrm{SF} = \mathrm{Facilitation}_{\mathrm{Release}} = (\mathrm{FCT})^4 \quad (9)$$

Note that this equation neglects the inevitable saturation of synaptic response, which would occur at sufficiently high levels of $[Ca^{2+}]$. Further, the cooperativity value of 4 lies at the high end of experimental

range obtained for the crayfish NMJ (Landò and Zucker, 1994; Wright et al., 1996; Ravin et al., 1999; Vyshedskiy and Lin, 2000). Therefore, all facilitation estimates in this paper are to be understood as *upper bounds* on physiologically attainable facilitation.

Based on experimental observations, we require a five-pulse SF magnitude of about 18-20 (see Figs. 1 *C* and 2 *C* of Tang et al., 2000). This corresponds to FCT of $P_5 / P_1 \sim 2.1$ (since $2.1^4 \sim 19.4$). Therefore, in the contour plots of Figs. 3 and 5, the parameter region yielding physiological magnitude of SF lies within the area bounded by the contour of FCT=2.0.

FCT grows with increasing distance between Ca^{2+} channel cluster and release site

There is substantial evidence for a close association between the vesicle release machinery and the presynaptic Ca^{2+} channels, suggesting their mutual proximity at many synapses (for reviews, see Stanley, 1997; Sheng et al., 1998; Catterall, 1999; Fisher and Bourque, 2001; Jarvis and Zamponi, 2001). At the crayfish NMJ, morphological studies suggest that vesicles are clustered along the edge of the AZ (Cooper et al., 1996; Atwood et al., 1997; Atwood and Karunanithi, 2002). However, at certain synapses, like the calyx of Held, vesicles may be scattered at various distances from the Ca^{2+} channel cluster (Meinrenken et al., 2002; Sätzler et al., 2002). Further, recent experiments on the sensitivity of phasic response to an application of a fast exogenous buffer (BAPTA) suggest that there is a significant separation between Ca^{2+} channels and secretion triggers at several strongly facilitating, but not at depressing, neocortical and hippocampal synapses (Rozov et al., 2001; Blatow et al., 2003). For any synapse type, it is possible that various obstacles to diffusion (such as vesicles themselves) and the tortuosity effects associated with the dense cytoskeletal and protein mesh within the AZ may significantly increase the effective diffusional distance between the Ca^{2+} channel and the release-triggering Ca^{2+} sensor. Therefore, we simulated the Ca^{2+} transients at various distances from the Ca^{2+} influx region. Figure 6 *A* demonstrates that the magnitude of FCT is increased by an increase in the channel-sensor separation. This result is easy to understand, because the buffer is able to bind more Ca^{2+} when it is acting over a longer diffusional distance (see review by Neher, 1998b), and thereby is more effective in reducing the first response, P_1, leading to higher FCT. Sufficient SF is achieved at distances of at least 40-60 nm from the Ca^{2+} channel cluster.

Facilitation growth is supralinear

As discussed above, Figs. 5 and 6 *A* demonstrate that the physiological magnitude of five-pulse SF

can be achieved within a certain range of values of k_{on} and B_{total} (K_D). However, we also need to establish whether BSM can reproduce the supralinear accumulation time course of SF observed at the crayfish NMJ (Figs. 1 *C* and 2 *C* of Tang et al., 2000; Fig. 2 *C* of Winslow et al., 1994). Traces in Fig. 6 *B* show that the simulated growth of FCT for a chosen parameter point (marked by an asterisk in Fig. 6 *A*) is indeed supralinear, at all distances from the Ca^{2+} channel cluster, and therefore facilitation of release (Eq. 9) grows supralinearly as well, in agreement with experiment. Figure 7 *A* demonstrates the supralinear time course of SF corresponding to the [Ca^{2+}] trace shown Fig. 6 *Bb*, yielding a physiological SF magnitude. In fact, we find that, for a mobile buffer, the parameter region yielding high facilitation coincides with the region of high supralinearity (data not shown). Therefore, BSM can successfully reproduce the SF magnitude and its accumulation time course observed experimentally at the crayfish NMJ.

Effect of exogenous buffers on facilitation growth.

The experimental observations of the reduction of SF by exogenously applied buffers were crucial for establishing the role of residual Ca^{2+} in SF (see review by Zucker and Regehr, 2002), and a successful SF model should reproduce this property. Figure 7 *A* shows the simulated effect of application of 200 μM of Fura-2, a fast and high-affinity mobile buffer, on SF magnitude, for a set of parameter values marked by an asterisk in Fig. 6 *Ab*. These simulation results agree very well with the experimental results of Tang et al. (2000) (Fig. 7 *B*). However, due to the non-monotonic dependence of FCT on B_{total}, adding a mobile high-affinity buffer may actually increase FCT, and hence SF, under certain conditions. Such paradoxical effect of exogenous buffers on SF has been termed “pseudofacilitation” (Neher, 1998a; Rozov et al., 2001; Blatow et al., 2003; see also Discussion).

FCT at lower buffer mobility.

Until now we have assumed that the Ca^{2+} buffer is highly mobile, with a diffusion coefficient comparable to that of ATP, BAPTA or EGTA (Naraghi and Neher, 1997). There are several studies that agree with such high mobility of endogenous buffers, for instance the experiments at goldfish retinal bipolar cells (Burrone et al., 2002), Purkinje cells (Maeda et al., 1999), and frog saccular hair cells (Roberts, 1993). However, endogenous buffers were found to be immobile or poorly mobile in many other preparations, including the calyx of Held (Helmchen et al., 1997), neocortical and hippocampal pyramidal cells (Helmchen et al, 1996; Ohana and Sakmann, 1998; Lee et al., 2000), axons of Aplysia neurons (Gabso et al., 1997), and bovine adrenal chromaffin cells (Neher and Augustine, 1992; Zhou and Neher, 1993; Xu et al., 1997). At the crayfish NMJ, the mobility of endogenous Ca^{2+} buffers is not known. To

study the dependence of the BSM on buffer mobility, we repeated our simulations for variable values of B_{total} and the D_B, the only parameter in Table 2 yet to be varied, for fixed values of κ_0 and k_{on} (κ_0 =500, k_{on}=0.8 $\mu M^{-1}ms^{-1}$). Figure 8 *A* shows that FCT declines dramatically as D_B is decreased, which agrees with the conditions for high FCT that were formulated in the first subsection of Results. At the same time, there is an increase in the optimal buffer concentration required to achieve maximal FCT. This is because a buffer with lower mobility is saturated much more readily, so greater B_{total} is required to prevent over-saturation. However, we find that the transition to the fixed buffer case (D_B= 0) is non-monotonic, and FCT starts increasing as D_B drops below about $0.01\mu m^2ms^{-1}$ (Fig. 8 *B*), suggesting the existence of a distinct facilitation regime at very low values of D_B.

FCT in the fixed buffer case.

At low mobility and high B_{total} it becomes possible for the buffer to absorb most of the Ca^{2+} influx before it reaches the Ca^{2+} sensor, strongly decreasing the first few responses, and thereby leading to a high FCT magnitude. This regime is most pronounced when the buffer is completely immobile; as Fig. 8 *B* shows, FCT rapidly decreases even for small non-zero values of D_B. Figure 9 *A* illustrates the behavior of FCT for D_B = 0, as a function of k_{on} and B_{total} (= 500 K_D), at different distances from the Ca^{2+} channel cluster (compare with the mobile buffer case, Fig. 6). FCT is seen to be relatively weakly dependent on k_{on}, for sufficiently high values of k_{on}. This is because the effective diffusional distance from the point of influx to the Ca^{2+} sensor is significantly increased in the presence of a fixed buffer, assuring that the Ca^{2+} ions will undergo multiple binding-unbinding steps for a wide range of k_{on} values. For this reason, FCT is sensitive to the buffer affinity, K_D, and not to k_{on}, as in the mobile buffer case. Therefore, FCT is also sensitive to the value of buffering capacity, κ_0. We find that large κ_0 is required to achieve high FCT in the fixed buffer case (data not shown).

The $[Ca^{2+}]$ traces shown in Fig. 9 *B* demonstrate that the free $[Ca^{2+}]_{res}$ makes a more significant contribution to Ca^{2+} peaks, as compared to the case of a mobile buffer (cf. Fig. 6 *B*). In fact, we find that the regions of high FCT and high free $[Ca^{2+}]_{res}$ significantly overlap (data not shown). When $[Ca^{2+}]_{res}$ is non-negligible, Eq. 9 should be modified to include its contribution to facilitation:

$$\text{Facilitation}_{\text{Release}} = ((P_5 + R_4) / P_1)^4 = (\text{FCT} + R_4 / P_1)^4 \qquad (10)$$

where R_4 equals $[Ca^{2+}]_{res}$ achieved at the end of the fourth inter-pulse interval (see Fig. 9 *Bb*). The R_4/P_1 ratio should remain much smaller than one, since the delayed asynchronous release 10 ms after the fourth pulse is known to be much smaller than the peak synaptic response achieved during the first pulse. The contribution of $[Ca^{2+}]_{res}$ increases with increasing B_{total} (K_D), and with increasing distance from the Ca^{2+} channel cluster. In fact, for sufficiently high B_{total} values and at large distances, the fast Ca^{2+} transient becomes completely shunted by the buffer, and the peak in Ca^{2+} concentration is significantly delayed with respect to the end of the pulse (in Fig. 9 *Bc*, the delay is 1.5 ms). Under these conditions the BSM would predict a physiologically unrealistic latency between the end of the Ca^{2+} influx and the peak of neurotransmitter release. At a given distance, there is only a narrow range of B_{total} values where the magnitude of facilitation (Eq. 10) reaches experimentally observed levels, while the free $[Ca^{2+}]_{res}$ contribution remains small ($R_4/P_1 \leq 0.2$). For a distance of 60 nm (Fig. 9 *Ab*), the corresponding range is about 10-12 mM, approaching unphysiologically high concentrations.

Figure 10 demonstrates the spatial distribution of the Ca^{2+} ions and the buffer at different times after the cessation of an AP, for a parameter point marked with a '+' in Fig. 9 *A*. Contrary to the mobile buffer case, it takes tens of milliseconds rather than a fraction of one millisecond for the concentrations to re-equilibrate in space, so the free $[Ca^{2+}]_{res}$ elevation and the buffer saturation region are still significantly localized by the end of a 10 ms-long interpulse interval. This illustrates that it is a *local* rather than *global* buffer saturation that underlies FCT in the fixed buffer case.

Further, we find that the accumulation time course of SF is sublinear for a fixed buffer. Figure 9 *Bb* shows the $[Ca^{2+}]$ trace, and Fig. 11 depicts the corresponding SF growth time course at a distance of 60 nm from the edge of the Ca^{2+} influx region, for a parameter point marked with a '+' in Fig. 9 *Ab*. In fact, we find that the SF accumulation time-course remains sublinear for any choice of parameter values (data not shown).

Facilitation decay time course and the effect of Fura-2 on facilitation decay.

Above we have shown that high buffer mobility is important for the BSM to explain the experimentally observed supralinear accumulation time-course of SF. For a highly mobile buffer, the Ca^{2+} concentration rapidly re-equilibrates throughout the terminal upon termination of the Ca^{2+} influx caused by an AP. Therefore, the buffer has to become saturated globally (i.e. in the entire presynaptic bouton) to cause significant FCT. The decay time course of facilitation will therefore be determined by the

extrusion of Ca^{2+} by the plasmalemma transport proteins, with possible contribution of uptake into internal Ca^{2+} stores. Since we were interested in establishing an upper bound on maximal SF magnitude that can be achieved by the BSM, we made a conservative assumption about the Ca^{2+} extrusion rate in our simulations, choosing a clearance time estimate of 5 sec, based on the crayfish NMJ measurements of Tank et al. (1995). This is much longer than the time scales of tens and hundreds of milliseconds that characterize the two components of SF decay observed at this synapse. The above estimate of Ca^{2+} clearance rate was obtained by tracking [Ca^{2+}] for tens of seconds after cessation of stimulation, when Ca^{2+} is low and the main mode of extrusion is through ATP-driven pumps. It is likely that immediately after stimulation the clearance proceeds at a faster rate, in particular due to activation of a lower-affinity but higher-capacity Na^{+}/Ca^{2+} exchanger, or some other low-affinity Ca^{2+} removal mechanism (e.g., a slow low-affinity buffer). Indeed, the decay of Ca^{2+} transients induced by AP trains was recently measured at the crayfish NMJ by Vyshedskiy and Lin (2000) on a finer time scale, revealing a bi-phasic decay with time constants of 84±30 and 390±153 ms. These time constants are comparable to the F1 (18±5ms) and F2 (530±200 ms) components of facilitation decay at the crayfish NMJ (Zucker, 1974; Vyshedskiy and Lin, 1997; Tang et al., 2000). Note that due to the non-linear dependence of transmitter release on Ca^{2+}, the SF decay times are expected to be somewhat shorter than the corresponding Ca^{2+} clearance time constants. Therefore, within the BSM framework, the decay time course of SF could be explained by the fast extrusion of Ca^{2+} from the terminal.

To allow for a faster decay of Ca transients, we have increased the pump dissociation constant from K_P=0.2μM to K_P=5μM, which is comparable to the affinity of the Na^{+}/Ca^{2+} exchanger (Blaustein and Lederer, 1999; Carafoli, 1987; DiPolo and Beauge, 1983), and increased the maximal extrusion rate from M=0.01 μM μm ms^{-1} to M=5 μM μm ms^{-1} (see Eq. 5). Figure 12 *A* shows the resulting SF decay time course, with and without additional Fura-2. Note that our simulations predict a slowing of SF decay in the presence of an exogenous buffer such as Fura-2, contrary to experimental observations (cf. Fig. 12 *C*). The slower decay is explained by the fact that the Ca^{2+} clearance time is directly proportional to the total intra-terminal buffering capacity (Neher and Augustine, 1992), which is approximately doubled after addition of 200 μM of Fura-2. We verified that this effect is maintained if we assume that the Fura-2 is immobilized (Matveev et al., 2002), and in simulations where decay of Ca^{2+} transients is caused by a slow endogenous buffer (data not shown).

One may suggest therefore that the observed decay properties of SF are more consistent with a model relying on the saturation of a *fixed* buffer: as discussed above, it is a local rather than global saturation that

causes FCT when buffers are fixed. Indeed, Figs. 10 and 9 *B* demonstrate that in the fixed buffer case the Ca^{2+} transients contain a gradually decaying (τ~10 ms) component caused by the slow spatial re-equilibration of Ca^{2+}, which is absent in the case of a mobile buffer (cf. Figs. 6 *B*). As we have shown previously (Matveev et al., 2002), this local free $[Ca^{2+}]_{res}$ is responsible for SF in the two-site model of Tang et al. (2000). In the BSM framework, it partially contributes to SF by adding to the Ca^{2+} transients (Fig. 9 *Bb*; Eq. 10). Therefore, in the presence of fixed buffers the SF decay is expected to contain a fast (F1-like) phase due to the spatial re-equilibration of Ca^{2+}, which should be strongly reduced in the presence of a mobile high-affinity Ca^{2+} buffer such as Fura-2, in agreement with experiment (Fig. 12 *B*). However, the second decay phase is slowed down in our simulations, as in the mobile buffer case (cf. Fig. 12 *A*). Thus, the model in its present form cannot successfully explain the experimentally observed effect of exogenous buffers on the decay time of SF, shown in Fig. 12 *C* (but see the Discussion below).

FCT in the presence of two buffers.

In this work we have concentrated on the case whereby a single dominant endogenous buffer is shaping the intracellular Ca^{2+} dynamics. We believe that a thorough investigation and understanding of the single-buffer situation is necessary before considering more complicated scenarios. However, one cannot exclude the possibility that several endogenous buffers make a commensurate contribution to the overall buffering capacity at the crayfish NMJ, as well as at other synapses. In particular, one may propose that the immobile or poorly mobile buffer with low capacity (κ_0~40-50) found in different cell types (references cited in Results) represents the basal buffer present in all synapses, while only a subset of cell types possess an additional mobile high-capacity buffer (e.g., calbindin; Nägerl et al., 2000). Although the data on the properties of the putative immobile low-capacity buffer is lacking, evidence from chromaffin cell studies suggest that it may have low affinity (Xu et al., 1997). Therefore, to analyze this possibility we performed simulations in which a mobile buffer with varying B_{total} and k_{on} was added to a fixed concentration of a low-affinity immobile buffer with B_{total}=750 μM, K_D=15 μM (κ_0=50), and k_{on}=0.1 $\mu M^{-1}ms^{-1}$ (Fig. 13). Our results show that the FCT is reduced when the low-affinity buffer is introduced, and that the size of this reduction depends on the relative capacities of the two buffers. Namely, the maximal achievable FCT is more significantly reduced when the immobile and mobile buffers have equal capacities (Fig. 13 *B*), whereas the FCT reduction is less dramatic when the capacity of the mobile buffer is significantly higher than the capacity of the low-affinity fixed buffer (Fig. 13 *A*). In general, we could not find conditions under which a two-buffer system would yield a higher FCT

magnitude as compared to a single buffer system (data not shown). This puts an additional emphasis on the point that the FCT magnitude that we demonstrate is the maximal bound on the FCT that can be achieved under physiological conditions.

DISCUSSION

Using a computer model of a crayfish motor bouton, we have explored in detail the phenomenon of facilitation of Ca^{2+} transients (FCT) resulting from the saturation of an endogenous Ca^{2+} buffer. We have given an exhaustive characterization of the dependence of FCT on the endogenous buffering parameters (Table 2), and have described the conditions necessary to obtain a sufficiently high SF magnitude, as summarized below. The requirement of significant distance between the Ca^{2+} source and the secretion site; our findings on the non-monotonic dependence of FCT on buffer concentration; and the increase of FCT with increasing $[Ca^{2+}]_{ext}$, are all consistent with the experimental results of Blatow et al. (2003).

Further, we compare our simulation results with the properties of SF observed at the crayfish NMJ by Tang et al. (2000). The crayfish NMJ is particularly well suited for the study of SF, since it displays pronounced SF under physiological conditions, and the increase of synaptic response is not occluded by concomitant synaptic depression, which is the case in most other systems (reviewed by Zucker and Regehr, 2002).

FCT and buffer mobility

As we have shown, buffer mobility is a crucial factor in the BSM. Curiously, we found that to achieve a physiologically relevant SF magnitude, the buffer has to be either highly mobile or highly immobilized, with much smaller FCT achieved for intermediate values of mobility (Fig. 8 *B*). This is because the mechanism by which buffer saturation causes facilitation is different in the high- vs. low-mobility regimes. A highly mobile buffer efficiently carries Ca^{2+} ions away from the AZ, strongly shunting the response to the first pulses in a stimulation train, while becoming gradually saturated in the entire bouton (Fig. 2). This results in large FCT. A fixed buffer causes facilitation by saturating locally, rather than globally, which traps Ca^{2+} ions in an area surrounding the AZ (Fig. 10; Nowycky and Pinter, 1993; Neher, 1998a). To absorb a significant fraction of the Ca^{2+} influx locally, the buffer has to be completely immobile, and its concentration has to be much higher than in the mobile buffer case, extending into the range of unrealistically high values (Figs. 8 *B*, 9). Further, achieving high saturation also requires a significant separation between the Ca^{2+} sensor and the Ca^{2+} source. However, at larger distances and higher B_{total}, the free $[Ca^{2+}]_{res}$ becomes comparable in magnitude to the fast Ca^{2+} transients, providing a

greater contribution to the over-all facilitation (Eq. 10). At large enough values of distance and B_{total}, the peak in Ca^{2+} concentration becomes significantly delayed with respect to the end of the Ca^{2+} influx (Fig. 9 *Bc*), since diffusion is slowed by the fixed buffer, and the trapped Ca^{2+} ions undergo multiple binding/unbinding steps before they reach their secretory target. Under these conditions, a single release site model is no longer consistent with the transient nature of the postsynaptic response. Therefore, the model would have to be expanded to include a proximal secretory trigger, in addition to the more distal facilitation site, as proposed by Tang et al. (2000) and explored more recently by Matveev et al. (2002). The proximal site would preserve the transient nature of transmitter release, since sufficiently close to the channel cluster the decay of Ca^{2+} peaks is fast.

In the present simulations, in the fixed buffer case the mechanism of facilitation undergoes a gradual qualitative change as the parameters are varied, and at high values of distance and B_{total}, the accumulation of free $[Ca^{2+}]_{res}$ becomes the principle source of facilitation (Fig. 9 *Bc*). For intermediate values of parameters, buffer saturation begins to contribute to the overall facilitation magnitude (Fig. 9 *Bb*). In contrast, in the mobile buffer case the FCT through buffer saturation represents the only mechanism of SF for a wide range of buffering conditions. These results further illustrate the opposing effects of fixed and mobile buffers on Ca^{2+} dynamics, elucidated in earlier studies (Junge and McLaughlin, 1987; Sala and Hernández-Cruz, 1990; Zhou and Neher, 1993; Nowycky and Pinter, 1993; Winslow et al., 1994; Gabso et al., 1997; Naraghi and Neher, 1997; Neher, 1998a).

Non-monotonic dependence on buffer concentration

Most studies show a reduction in SF upon introduction of exogenous mobile Ca^{2+} buffers, pointing to the importance of residual Ca^{2+} as the main source of SF (reviewed in Zucker and Regehr, 2002). Our results suggest that this effect is consistent with the BSM (Figs. 7, 11-12). However, depending on whether the endogenous buffering conditions correspond to the "ascending" or the "descending" slope of the FCT peak in Fig. 3, and depending on the mobility of the added buffer relative to the endogenous one, one would predict either an increase or a decrease in the facilitation magnitude. Further, regardless of the source of SF under physiological conditions, adding an alien mobile Ca^{2+} buffer may change the physiological mechanism of facilitation to that of FCT. Such "pseudofacilitation" (Neher, 1998a) may turn out to be greater in magnitude than the native facilitation under control conditions, but as Fig. 3 suggests, it would inevitably decline as the concentration of the added buffer is ramped up sufficiently. This agrees completely with the "pseudofacilitation" effect that has been observed at some neocortical and

hippocampal synapses in response to BAPTA application (see Fig. 9 *B* in Rozov et al., 2001, and Fig. 3 *B* of Blatow et al., 2003). Pseudofacilitation may also explain the discrepancy between the results of Winslow et al. (1994), showing the lack of effect of BAPTA-AM on facilitation at the crayfish NMJ, and the results of other studies showing that similar manipulations reduce facilitation in this system. It may be argued that the particular concentration of BAPTA-AM used by Winslow et al. caused a pseudofacilitation effect that balanced the concomitant reduction of facilitation occurring through a different mechanism (see also Discussion in Bennett et al., 2000).

Dependence on external Ca^{2+} concentration

The dependence of FCT on the buffer concentration (and hence, on its affinity K_D, as well) remains non-monotonic, even if the value of κ_0 is kept fixed (Figs. 5, 6 *A*, 9 *A*). It follows then that the dependence of FCT on I_{Ca} is also non-monotonic, since changing the value of I_{Ca} is equivalent to a simultaneous rescaling of the parameters B_{total} and K_D in the opposite direction (Figs. 3 *A*, 5 *A*). A consequence of this fact is that the FCT is an increasing function of the external Ca^{2+}, $[Ca^{2+}]_{ext}$, for small enough values of $[Ca^{2+}]_{ext}$, assuming that I_{Ca} is proportional to $[Ca^{2+}]_{ext}$. This agrees with the experimental results of Blatow et al. (2003) and Rozov et al. (2001). However, at sufficiently high values of $[Ca^{2+}]_{ext}$, the dependence of SF on $[Ca^{2+}]_{ext}$ should reverse. Further, the saturation of the putative secretory site and the potential emergence of short-term synaptic depression at higher release rates, two effects not included in our model, would limit the range of $[Ca^{2+}]_{ext}$ values for which SF grows with $[Ca^{2+}]_{ext}$.

Dependence on the properties of the release mechanism

As discussed above, we have chosen to quantify facilitation solely in terms of the increase in the Ca^{2+} concentration. Inclusion of a specific Ca^{2+}-dependent vesicle release scheme would obscure the relationship between the facilitation magnitude and the Ca^{2+}-binding properties of the buffer. Saturation of the release mechanism at high $[Ca^{2+}]$ would reduce SF estimates calculated according to Eqs. 9 and 10, especially at low values of B_{total} and k_{on}, and for small separations between the Ca^{2+} channel and the release site, since these conditions correspond to high Ca^{2+} concentration. Therefore, saturation effects would move the FCT peak in parameter sweep plots of Figs. 3, 5-6, 8-9 to higher values of B_{total}, and the height of the peak may be significantly reduced. However, all our conclusions about the qualitative

dependence of FCT on the endogenous buffering parameters would remain unchanged.

Facilitation accumulation time course

We have found that the saturation of either a very mobile or a completely immobilized buffer may explain the magnitude of SF observed at the crayfish NMJ (Figs. 7, 11). However, the observed supralinear accumulation time course of SF is only predicted if the endogenous buffer is mobile. In agreement with our results, experiments of Blatow et al. (2003) reveal a supralinear SF growth at a hippocampal mossy fiber synapse that contains a highly mobile calbindin (see Fig. 5 *C* therein; properties of calbindin have been described by Nägerl et al., 2000). Note also that lowering the assumed Ca^{2+}-cooperativity of release from 4 to 3, and including saturation at high Ca^{2+} levels, would make the simulated SF growth less steep, favoring even more the mobile buffer model over the fixed buffer case.

It is important to bear in mind that our results show the *upper bound* on the physiologically attainable level of SF. Therefore, even in the more favorable mobile buffer case, the parameter region corresponding to the observed magnitude of SF may be more narrow than our results in Figs. 3, 5, 6 and 13 suggest, in particular because we assume very high buffer mobility and a non-saturating relationship between transmitter release and $[Ca^{2+}]$.

Acceleration of facilitation decay by exogenous buffers

Although saturation of a mobile buffer can successfully explain the observed magnitude and accumulation time course of SF, we showed that it is not consistent with the observed acceleration of decay of SF by fast high-affinity exogenous buffers (Fig. 12 *A, C*). In the fixed buffer case, the faster phase of decay, corresponding to the spatial re-equilibration of the locally elevated residual Ca^{2+}, would be indeed accelerated upon adding a mobile buffer. Still, the slower decay phase, corresponding to Ca^{2+} clearance, would be slowed down, as in the mobile buffer case (Fig. 12 *B*). However, one may suggest that a slow leak of Ca^{2+} from the bouton into the axonal compartment, an effect not included in our model, may make a significant contribution to the decay of SF. If the mobility of the exogenous buffer is greater than or equal to the mobility of the endogenous one, then its addition would accelerate the putative leak of Ca^{2+} into the axon, thereby accelerating SF decay. It is not clear however whether the faster decay of both components of SF could be explained by this leak mechanism. Further, recent crayfish NMJ experiments by J.-Y. Lin, Q. Fu and T. Allana (in preparation) show that the decay of Ca^{2+} transients on time scales of tens to hundreds of milliseconds is not sensitive to the mobility of the Ca^{2+}-sensitive dye used to image $[Ca^{2+}]$, arguing against the importance of this leak. The above study also suggests that the

endogenous Ca buffers at the crayfish opener NMJ are characterized by low mobility. Therefore, it is unlikely that BSM can explain the observed properties of SF at the crayfish NMJ. However, further modeling work that would incorporate this new experimental data is necessary to reach a definite conclusion. Parenthetically, we note that at the frog NMJ, addition of exogenous buffer does slow the decay of SF (Robitaille and Charlton, 1991), as predicted by the present model.

We showed previously (Matveev et al., 2002) that both the growth and the decay properties of SF at the crayfish NMJ can be explained by a model with a distant facilitation site proposed by Tang et al. (2000). However, to explain the supralinear accumulation time-course, the two-site model had to incorporate additional assumptions of a very large separation between the SF sensor and the Ca^{2+} channel array (> 250 nm), or a high degree of tortuosity near the active zone. The two-site model is similar to the BSM in that both rely exclusively on the dynamics of Ca^{2+} diffusion and buffering to explain the observed behavior of SF, in particular its decay time course. An alternative possibility is that at least one of the facilitation decay components may result from the slow unbinding of Ca^{2+} from a release-controlling Ca^{2+} sensor (Yamada and Zucker, 1992; Bertram et al., 1996; Bennett et al., 1997; Dittman et al., 2000). In its pure form, such a *bound* Ca^{2+} model is inconsistent with experimental data demonstrating the importance of free residual Ca^{2+} for SF (reviewed in Zucker and Regehr, 2002). Yet it is possible that a hybrid model, sensitive to free Ca^{2+} but including a slow unbinding process, could also reproduce the facilitation behavior observed at the crayfish NMJ. Although recent experiments have ruled out the existence of a slow unbinding step at the calyx of Held terminal (Felmy et al., 2003), it was shown to play a role at a cerebellar granule cell synapse (Atluri and Regehr, 1996).

Our analysis shows that the buffer saturation mechanism (better termed the FCT model) and the two-site residual free Ca^{2+} model can be viewed as being on the opposite sides of the same spectrum (Fig. 8 *B*). Whereas the FCT is most pronounced when a highly *mobile* buffer saturates *globally*, the accumulation of free $[Ca^{2+}]_{res}$ is mediated by the *local* saturation of (local Ca^{2+} trapping by) a high-concentration *fixed* buffer. However, there exists an intermediate parameter regime, where the accumulation of free $[Ca^{2+}]_{res}$ and the facilitation of Ca^{2+} transients can both contribute to synaptic facilitation (Fig. 9 *Bb*).

APPENDIX

The case of non-zero resting Ca^{2+} concentration.

Although our simulations assume zero resting Ca^{2+} concentration, Ca_{rest}, the results can be straightforwardly translated to the case of non-zero Ca_{rest}. The Ca_{rest} is a constant term not affecting the dynamics of diffusion or buffering, so its effect is limited to a transformation of model parameters. Let's express the total $[Ca^{2+}]$ as a sum of Ca_{rest} and the contribution due to Ca^{2+} entry during an action potential ($[Ca^{2+}] \equiv [Ca^{2+}]_{AP}$): $[Ca^{2+}]_{total} = Ca_{rest} + [Ca^{2+}]$. Since the derivative of the constant resting term Ca_{rest} on the left- and the right-hand sides of Eq. 2 is zero, the only change is in the reaction term on the right-hand side of Eqs. 2 and 3:

$$R = - k_{on} [B] [Ca^{2+}] + k_{off} (B_{total} - [B]) \tag{11}$$

Let us now introduce the resting concentration of free buffer, B_{rest}, in equilibrium with the resting Ca^{2+}:

$$k_{on}\, Ca_{rest}\, B_{rest} = k_{off} (B_{total} - B_{rest}) \tag{12}$$

$$\mathrm{B_{rest}} = \frac{\mathrm{B_{total}\, K_D}}{\mathrm{Ca_{rest} + K_D}}, \quad \text{where } \mathrm{K_D} = \frac{\mathrm{k_{off}}}{\mathrm{k_{on}}} \tag{13}$$

We can then express the reaction term as

$$R = - k_{on} [B] (Ca_{rest} + [Ca^{2+}]) + k_{off} (B_{total} - B_{rest}) + k_{off} (B_{rest} - [B]) \tag{14}$$

Using Eq. 12 to eliminate the second term in above expression, this yields

$$R = - k_{on} [B] (Ca_{rest} + [Ca^{2+}]) + k_{on}\, Ca_{rest}\, B_{rest} + k_{off} (B_{rest} - [B]) =$$

$$= - k_{on} [B] [Ca^{2+}] + (k_{off} + k_{on}\, Ca_{rest}) (B_{rest} - [B]) \tag{15}$$

Now, notice that the reaction term has the same form as in the Ca_{rest}=0 case (Eq. 11), except that B_{total} has to be replaced with B_{rest} (given by Eq. 13), and k_{off} has to be replaced with $k_{off} + k_{on}\, Ca_{rest}$, which in turn implies that K_D has to be replaced with $K_D + Ca_{rest}$. Note that this parameter transformation allows us to recover the expression for the rest-state buffering ratio κ_0 in the non-zero Ca_{rest} case (Eq. 6):

$$\kappa_0 = \frac{\mathrm{B'_{total}}}{\mathrm{K'_D}} = \frac{\mathrm{B_{rest}}}{\mathrm{K_D + Ca_{rest}}} = \frac{\mathrm{B_{total}\, K_D}}{(\mathrm{K_D + Ca_{rest}})^2} \tag{16}$$

where the primed parameters correspond to the case of zero Ca_{rest}. As expected, the value of the buffering ratio is invariant with respect to this parameter change.

Thus, to recover the dependence of facilitation on model parameters for the case of non-zero Ca_{rest},

the inverse of the above transformations has to be applied to the parameter values in Figs. 2-13:

$$B_{total} = \frac{B'_{total}}{1 - Ca_{rest}/K'_D}, \quad k_{off} = k'_{off}\left(1 - \frac{Ca_{rest}}{K'_D}\right), \quad K_D = K'_D - Ca_{rest} \tag{17}$$

where $K'_D > Ca_{rest}$. Note that the value of k_{on} remains unaltered by this substitution. The condition $K'_D > Ca_{rest}$ implies that the magnitude of Ca_{rest} imposes a constraint on the relevant range of values of K'_D. Given a certain value of Ca_{rest}, one should ignore those parts of Figs. 3, 5-6 and 13 that lie in the region $K'_D < Ca_{rest}$. The transformations described by Eq. (17) will have no effect on the results for the fixed buffer case (Fig. 9), since the value of K'_D is much greater than Ca_{rest} in the relevant parameter range. In the mobile buffer case, for the fixed-κ_0 plots showing the dependence of facilitation on B'_{total} (K'_D) and k_{on} (Figs. 5 and 6), these transformations involve a simple shift to the left by the amount equal to Ca_{rest}, after the abscissa values are re-interpreted in terms of K'_D instead of B'_{total}. Note that the constant-κ_0 proportionality relationship between K_D and B_{total} no longer holds in this case, but is determined according to Eq. 6:

$$B_{total} = \kappa_0 K_D (1 + Ca_{rest}/K_D)^2 \tag{18}$$

Assuming for example Ca_{rest}=0.1 μM, the facilitation peak in Figs. 5 *A* and 6 *Ab* at {k_{on}=1 $\mu M^{-1}ms^{-1}$, B'_{total}=400μM, K'_D=0.8 μM} corresponds to {B_{total}=457μM, K_D=0.7 μM}. In Fig. 3, where the values of B'_{total} and K'_D (k'_{on}) are independently varied, the transformation to the non-zero Ca_{rest} would involve a downward shift along the K'_D axis by Ca_{rest}, as well as a non-homogenous stretch to the right, shifting the facilitation peak to higher values of B_{total}. The latter shift in the B_{total} direction is more significant for lower values of K'_D. Further, the value of k_{off} will not remain constant throughout panels *A* and *B*, due to its dependence on K'_D (see Eq. 17). Thus, the independence of facilitation on the value of k_{off} in the mobile buffer case (Fig. 3) is only approximate, holding for values of $K_D >> Ca_{rest}$.

REFERENCES

Allbritton, N. L., T. Meyer, and L. Stryer. 1992. Range of messenger action of calcium ion and inositol 1,4,5-trisphosphate. *Science* 258:1812-1815.

Atluri, P. P., and W. G. Regehr. 1996. Determinants of the time course of facilitation at the granule cell to Purkinje cell synapse. *J. Neurosci.* 16:5661-5671.

Atwood, H. L., and S. Karunanithi. 2002. Diversification of synaptic strength: presynaptic elements. *Nat. Rev. Neurosci.* 3:497-516.

Atwood, H. L., S. Karunanithi, J. Georgiou, and M.P. Charlton. 1997. Strength of synaptic transmission at neuromuscular junctions of crustaceans and insects in relation to calcium entry. *Invert. Neurosci*. 3:81-87.

Bennett, M. R., W. G. Gibson, and J. Robinson. 1997. Probabilistic secretion of quanta and the synaptosecretosome hypothesis: evoked release at active zones of varicosities, boutons, and endplates. *Biophys. J.* 73:1815-1829.

Bennett, M. R., L. Farnell, and W. G. Gibson. 2000. The probability of quantal secretion within an array of calcium channels of an active zone. *Biophys. J.* 78:2222-2240.

Bertram, R., A. Sherman, and E. Stanley. 1996. The single domain/bound calcium hypothesis of transmitter release and facilitation. *J. Neurophysiol.* 75:1919-1931.

Blaustein, M. P., and W. J. Lederer. 1999. Sodium/calcium exchange: its physiological implications. *Physiol. Rev.* 79:763-854.

Blatow, M., A. Caputi, N. Burnashev, H. Monyer, and A. Rozov. 2003. Ca^{2+} buffer saturation underlies paired pulse facilitation in calbindin-D28k-containing terminals. *Neuron.* 38:79-88.

Bollmann, J. H., B. Sakmann, and J. G. Borst. 2000. Calcium sensitivity of glutamate release in a calyx-type terminal. *Science* 289:953-957.

Burrone, J., G. Neves, A. Gomis, A. Cooke, and L. Lagnado. 2002. Endogenous calcium buffers regulate fast exocytosis in the synaptic terminal of retinal bipolar cells. *Neuron.* 33:101-112.

Carafoli, E. 1987. Intracellular calcium homeostasis. *Ann. Rev. Biochem.* 56:395-433.

Catterall, W. A. 1999. Interactions of presynaptic Ca^{2+} channels and snare proteins in neurotransmitter release. *Ann. N. Y. Acad. Sci.* 868:144-159.

Chad, J. E., and R. Eckert. 1984. Calcium domains associated with individual channels can account for anomalous voltage relations of Ca-dependent responses. *Biophys. J.* 45:993-999.

Cooper, R. L., L. Marin, and H. L. Atwood. 1995. Synaptic differentiation of a single motor neuron: conjoint definition of transmitter release, presynaptic calcium signals, and ultrastructure. *J. Neurosci.* 15:4209-4222.

Cooper, R. L., J. L. Winslow, C. K. Govind, and H. L. Atwood. 1996. Synaptic structural complexity as a factor enhancing probability of calcium-mediated transmitter release. *J. Neurophysiol.* 75:2451-2466.

Delaney, K. R., and D. W. Tank. 1994. A quantitative measurement of the dependence of short-term synaptic enhancement on presynaptic residual calcium. *J. Neurosci.* 14: 5885-5902.

Dipolo, R., and L. Beauge. 1983. The calcium pump and sodium-calcium exchange in squid axons. Annu. Rev. Physiol. 45:313-324.

Dittman, J. S., A. C. Kreitzer, and W. G. Regehr. 2000. Interplay between facilitation, depression, and residual calcium at three presynaptic terminals. *J. Neurosci.* 20:1374-1385.

Felmy, F. E., E. Neher, and R. Schneggenburger. 2003. Probing the intracellular calcium sensitivity of transmitter release during synaptic facilitation. *Neuron.* 37:801-811.

Fisher, S. A., T. M. Fischer, and T. J.Carew. 1997. Multiple overlapping processes underlying short-term synaptic enhancement. *Trends Neurosci.* 20:170-177.

Fisher, T. E., and C. W. Bourque. 2001. The function of Ca^{2+} channel subtypes in exocytotic secretion: new perspectives from synaptic and non-synaptic release. *Prog. Biophys. Mol. Biol.* 77:269-303.

Fogelson, A. L., and R. S. Zucker. 1985. Presynaptic calcium diffusion from various arrays of single channels. Implications for transmitter release and synaptic facilitation. *Biophys. J.* 48:1003-1017.

Gabso, M., E. Neher, and M. E. Spira. 1997. Low mobility of the Ca^{2+} buffers in axons of cultured Aplysia neurons. *Neuron*. 18:473-481.

Helmchen, F., J. G. Borst, and B. Sakmann. 1997. Calcium dynamics associated with a single action potential in a CNS presynaptic terminal. *Biophys. J.* 72:1458-1471.

Helmchen, F., K. Imoto, and B. Sakmann. 1996. Ca^{2+} buffering and action potential-evoked Ca^{2+} signaling in dendrites of pyramidal neurons. *Biophys. J.* 70:1069-1081.

Hines, M. 1984. Efficient computation of branched nerve equations. *Int. J. Bio-Medical Computing* 15:69-76.

Irving, M., J. Maylie, N. L. Sizto, and W. K. Chandler. 1990. Intracellular diffusion in the presence of mobile buffers. Application to proton movement in muscle. *Biophys. J.* 57:717-721.

Jackson, M. B., and S. J. Redman. 2003. Calcium dynamics, buffering, and buffer saturation in the boutons of dentate granule-cell axons in the hilus. *J. Neurosci.* 23:1612-1621.

Jarvis, S. E., and G. W. Zamponi. 2001. Interactions between presynaptic Ca^{2+} channels, cytoplasmic messengers and proteins of the synaptic vesicle release complex. *Trends Pharmacol. Sci.* 22:519-525.

Junge, W., and S. McLaughlin. 1987. The role of fixed and mobile buffers in the kinetics of proton movement. *Biochim. Biophys. Acta.* 890:1-5.

Katz, B., and R. Miledi. 1968. The role of calcium in neuromuscular facilitation. *J. Physiol.* 195:481-92.

Keizer, J. 1987. Diffusion effects on rapid bimolecular chemical reactions. *Chem. Rev.* 87:167-180.

Klingauf, J., and E. Neher. 1997. Modeling buffered Ca^{2+} diffusion near the membrane: implications for secretion in neuroendocrine cells. *Biophys. J.* 72:674-690.

Landò, L., and R. S. Zucker. 1994. Ca^{2+} cooperativity in neurosecretion measured using photolabile Ca^{2+} chelators. *J. Neurophysiol.* 72:825-830.

Lee, S. H., C. Rosenmund, B. Schwaller, and E. Neher. 2000. Differences in Ca^{2+} buffering properties between excitatory and inhibitory hippocampal neurons from the rat. *J. Physiol.* 525:405-418.

Maeda, H., G. C. Ellis-Davies, K. Ito, Y. Miyashita, and H. Kasai. 1999. Supralinear Ca^{2+} signaling by cooperative and mobile Ca^{2+} buffering in Purkinje neurons. *Neuron* 24:989-1002.

Magleby, K. L. 1987. Short-term changes in synaptic efficacy. In: Synaptic function (Edelman G, Gall W, Cowan W, eds), pp 21-56. New York: Wiley.

Matveev, V., A. Sherman, and R. S. Zucker. 2002. New and corrected simulations of synaptic facilitation. *Biophys. J.* 83:1368-1373.

Meinrenken, C. J., J. G. Borst, and B. Sakmann. 2002. Calcium secretion coupling at calyx of Held governed by nonuniform channel-vesicle topography. *J. Neurosci.* 22:1648-1667.

Morton, K. W., and D. F. Mayers. 1994. Numerical solution of partial differential equations: an introduction. University Press, Cambridge.

Nägerl, U. V., D. Novo, I. Mody, and J. L. Vergara. 2000. Binding kinetics of calbindin-D(28k) determined by flash photolysis of caged Ca^{2+}. *Biophys. J.* 79:3009-3018.

Naraghi, M., and E. Neher. 1997. Linearized buffered Ca^{2+} diffusion in microdomains and its implications for calculation of $[Ca^{2+}]$ at the mouth of a calcium channel. *J. Neurosci.* 17:6961-6973.

Neher, E. 1998a. Usefulness and limitations of linear approximations to the understanding of Ca^{++} signals. *Cell Calcium* 24:345-357.

Neher, E. 1998b. Vesicle pools and Ca^{2+} microdomains: new tools for understanding their roles in neurotransmitter release. *Neuron* 20:389-399.

Neher, E., and G. J. Augustine. 1992. Calcium gradients and buffers in bovine chromaffin cells. *J. Physiol.* 450:273-301.

Nowycky, M. C., and M. J. Pinter. 1993. Time courses of calcium and calcium-bound buffers following calcium influx in a model cell. *Biophys. J.* 64:77-91.

Ohana, O., and B. Sakmann. 1998. Transmitter release modulation in nerve terminals of rat neocortical pyramidal cells by intracellular calcium buffers. *J. Physiol.* 513:135-148.

Ohnuma, K., M. D. Whim, R. D. Fetter, L. K. Kaczmarek, and R. S. Zucker. 2001. Presynaptic target of

Ca^{2+} action on neuropeptide and acetylcholine release in *Aplysia californica*. *J. Physiol.*535:647-662.

Pape, P. C., D.-S. Jong, and W. K. Chandler. 1998. Effects of partial sarcoplasmic reticulum calcium depletion on calcium release in frog cut muscle fibers equilibrated with 20 mM EGTA. *J. Gen. Physiol.* 112:263-295.

Rahamimoff, R. 1968. A dual effect of calcium ions on neuromuscular facilitation. *J. Physiol.* 195:471-480.

Ravin, R., H. Parnas, M. E. Spira, N. Volfovsky, and I. Parnas. 1999. Simultaneous measurement of evoked release and [Ca^{2+}]i in a crayfish release bouton reveals high affinity of release to Ca^{2+}. *J. Neurophysiol.* 81:634-642.

Regehr, W. G., K. R. Delaney, and D. W. Tank. 1994. The role presynaptic calcium in short-term enhancement at the hippocampal mossy fiber synapse. *J. Neurosci*. 14:523-537.

Roberts, W. M. 1993. Spatial calcium buffering in saccular hair cells. *Nature.* 363:74-76.

Roberts, W. M. 1994. Localization of calcium signals by a mobile calcium buffer in frog saccular hair cells. *J. Neurosci.* 14:3246-3262.

Robitaille R., and M. P. Charlton. 1991. Frequency facilitation is not caused by residual ionized calcium at the frog neuromuscular junction. *Ann. N. Y. Acad. Sci.* 635:492-494.

Rozov, A., N. Burnashev, B. Sakmann, and E. Neher. 2001. Transmitter release modulation by intracellular Ca^{2+} buffers in facilitating and depressing nerve terminals of pyramidal cells in layer 2/3 of the rat neocortex indicates a target cell-specific difference in presynaptic calcium dynamics. *J. Physiol.* 531:807-826.

Sala, F., and A. Hernández-Cruz. 1990. Calcium diffusion modeling in a spherical neuron. Relevance of buffering properties. *Biophys. J.* 57:313-324.

Sätzler, K., L. F. Sohl, J. H. Bollmann, J. G. Borst, M. Frotscher, B. Sakmann, and J. H. Lubke. 2002. Three-dimensional reconstruction of a calyx of Held and its postsynaptic principal neuron in the medial nucleus of the trapezoid body. *J. Neurosci.* 22:10567-10579.

Schneggenburger, R., and E. Neher. 2000. Intracellular calcium dependence of transmitter release rates at a fast central synapse. *Nature* 406:889-893.

Sheng, Z. H., R. E. Westenbroek, W. A. Catterall. 1998. Physical link and functional coupling of presynaptic calcium channels and the synaptic vesicle docking/fusion machinery. *J. Bioenerg. Biomembr.* 30:335-345.

Simon, S. M., and R. R. Llinás. 1985. Compartmentalization of the submembrane calcium activity during calcium influx and its significance in transmitter release. *Biophys. J.* 48:485-498.

Smith, G. D., J. Wagner, and J. Keizer. 1996. Validity of the rapid buffering approximation near a point

source of calcium ions. *Biophys. J.* 70:2527-2539.

Smith, G. D., L.-X. Dai, R. Miura, and A. Sherman. 2001. Asymptotic analysis of equations for the buffered diffusion of intracellular calcium. *SIAM J. Applied Math.* 61:1816-1838.

Stanley, E. F. 1997. The calcium channel and the organization of the presynaptic transmitter release face. *Trends Neurosci.* 20:404-409.

Tang, Y., T. Schlumpberger, T. Kim, M. Lueker, and R. S. Zucker. 2000. Effects of mobile buffers on facilitation: experimental and computational studies. *Biophys. J.* 78:2735-2751.

Tank, D. W., W. G. Regehr, and K. R. Delaney. 1995. A quantitative analysis of presynaptic calcium dynamics that contribute to short-term enhancement. *J. Neurosci.* 15:7940-7952.

Trommershäuser, J., R. Schneggenburger, A. Zippelius, and E. Neher. 2003. Heterogeneous presynaptic release probabilities: functional relevance for short-term plasticity. *Biophys. J.* 84:1563-1579.

Vyshedskiy, A., and J.-W. Lin. 1997. Activation and detection of facilitation as studied by presynaptic voltage control at the inhibitor of the crayfish opener muscle. *J. Neurophysiol.* 77:2300-2315.

Vyshedskiy, A., and J.-W. Lin. 2000. Presynaptic Ca^{2+} influx at the inhibitor of the crayfish neuromuscular junction: a photometric study at a high time resolution. *J. Neurophysiol.* 83:552-562.

Winslow, J. L., S. N. Duffy, and M. P. Charlton. 1994. Homosynaptic facilitation of transmitter release in crayfish is not affected by mobile calcium chelators: implications for the residual ionized calcium hypothesis from electrophysiological and computational analyses. *J. Neurophysiol.* 72:1769-1793.

Wright, S. N., Brodwick, M. S., and Bittner, G. D. 1996. Calcium currents, transmitter release and facilitation of release at voltage-clamped crayfish nerve terminals. *J. Physiol.* 496:363-378.

Xu, T., M. Naraghi, H. Kang, and E. Neher. 1997. Kinetic studies of Ca^{2+} binding and Ca^{2+} clearance in the cytosol of adrenal chromaffin cells. *Biophys. J.* 73:532-545.

Yamada, W.M., and R. S. Zucker. 1992. Time course of transmitter release calculated from simulations of a calcium diffusion model. *Biophys. J.* 61:671-682.

Zhou, Z., and E. Neher. 1993. Mobile and immobile calcium buffers in bovine adrenal chromaffin cells. *J. Physiol.* 469:245-273.

Zucker, R. S. 1974. Characteristics of crayfish neuromuscular facilitation and their calcium dependence. *J. Physiol.* 241:91-110.

Zucker, R. S. 1994. Calcium and short-term synaptic plasticity. *Neth. J. Zool.* 44:495-512.

Zucker, R. S. 1996. Exocytosis: a molecular and physiological perspective. *Neuron* 17:1049-1055.

Zucker, R. S. 1999. Calcium- and activity-dependent synaptic plasticity. *Curr. Opin. Neurobio.* 9:305-313.

Zucker, R. S., and W. G. Regehr. 2002. Short-term synaptic plasticity. *Annu. Rev. Physiol.* 64:355-405.

LIST OF TABLES AND FIGURES

Table 1. Models of synaptic facilitation. Endogenous Ca^{2+} buffers play a crucial role in both (*2*) the residual free Ca^{2+} model and (*3*) the BSM. References: *(1)* Yamada and Zucker (1992), Bertram et al. (1996); see also Regehr et al. (1994), Atluri and Regehr (1996), Bennett et al. (1997), Dittman et al. (2000); *(2)* Tang et al. (2000), Matveev et al. (2002); *(3)* Klingauf and Neher (1997), Neher (1998a,b), Maeda et al. (1999), Blatow et al. (2003); see also Bennett et al. (2000), Rozov et al. (2001), Felmy et al. (2003), Jackson and Redman (2003), Trommershäuser et al. (2003).

Table 2. Free model parameters.

Figure 1. Model of a presynaptic crayfish motor bouton. The crayfish motor terminal is approximately represented as a sphere 3 μm in diameter (*bottom*), with active zones (AZs) distributed evenly over the spherical surface. Ca^{2+} diffusion and buffering are only simulated in the conical region of the sphere surrounding a single AZ. The ring of vesicles around the model AZ is shown for illustration only, and is not included in the simulation. Current density $g(\theta)$ (see Eqs. 2, 4) is assumed to be uniformly distributed over a disk surface area 160 nm in diameter (*top*). Asterisks mark the locations at which the Ca^{2+} concentration is sampled during the simulations. These sites represent locations of the putative Ca^{2+} "sensors" (possible vesicles locations). We record Ca^{2+} concentration 20 nm below the membrane surface, and at lateral distances of 20, 60 and 100 nm away from the edge of the Ca^{2+} current influx (corresponding sites are marked *1* through *3*).

Figure 2. Demonstration of the facilitation of Ca^{2+} transients caused by buffer saturation. Ca^{2+} (*middle panel*) and buffer (*bottom panel*) concentration time courses produced in response to a 5-pulse train of 1 ms-long Ca^{2+} current pulses (*top panel*), as measured at a distance of 60 nm from the edge of the Ca^{2+} channel cluster (site *2* in Fig. 1). The growth in the Ca^{2+} transient between the fifth and the first Ca^{2+} pulses, ΔP, depends on the degree of buffer saturation achieved right before (ΔB) and during (B_P) the final pulse. See text for details. Parameters are: B_{total}= 500 μM, K_D= 0.5 μM, k_{on} = 0.8 $\mu M^{-1}ms^{-1}$, D_B= 0.2 $\mu m^2 ms^{-1}$, I_{Ca}= 11.7 pA.

Figure 3. FCT as a function of buffer affinity and total buffer concentration. FCT is measured as the ratio

of the fifth and the first Ca^{2+} transients, P_5 / P_1, at a distance of 60 nm from the edge of the Ca^{2+} channel cluster (site *2* in Fig. 1), for (*A*) k_{off}=0.4 ms^{-1} and (*B*) k_{off}=0.1 ms^{-1}. The remaining parameter values are the same as in Fig. 2 (D_B = 0.2 $\mu m^2 ms^{-1}$, I_{Ca}=11.7 pA). FCT is constant along the contours separating the differently shaded bands, and its value is indicated on each of the contours. FCT grows with decreasing K_D (increasing k_{on}). Given a fixed value of K_D (k_{on}), maximal FCT is achieved at some finite value of B_{total}, denoted B^*_{total}. '+' mark the parameter points corresponding to panels *A* through *C* in Fig. 4. Note the similarity between data in panels *A* and *B*, and the equal range of k_{on} values in the two cases (scale on the right). The diagonal line marks the set of parameter points corresponding to $\kappa_0=B_{total}/K_D$=500. Increasing (decreasing) I_{Ca} is equivalent to sliding left (right) along this line (see text for details). For example, the value of FCT for $\tilde{I}_{Ca}$=5.85 pA, half the value used in this plot, at the parameter point corresponding to the filled circle (B_{total}=350 μM, K_D=0.7 μM), is equal to FCT for the doubled values of I_{Ca}, B_{total} and K_D (I_{Ca}=11.7 pA, B_{total}=700 μM, K_D=1.4 μM), corresponding to the open circle, yielding FCT≈1.8.

Figure 4. FCT in response to five Ca^{2+}-current steps, for three different values of the total buffer concentration (marked by '+' in Fig. 3 *A*): *(A)* B_{total}=200 μM, *(B)* B_{total}= B^*_{total}=500 μM, and *(C)* B_{total}= 1000 μM. Shown are [Ca^{2+}] (*upper* panels), and the buffer concentration (*bottom* panels) time courses. Notice the difference in scale along the concentration axis. The size of the first Ca^{2+} peak is scaled to the same level for easy comparison. FCT achieved in *B* is higher than in either *A* or *C*. Buffer affinity is K_D=0.5 μM (k_{on} = 0.8 $\mu M^{-1} ms^{-1}$), corresponding to the bottom edge of Fig. 3 *A*. Other parameters are the same as in Figs. 2 and 3 *A* (k_{off} = 0.4 ms^{-1}, D_B = 0.2 $\mu m^2 ms^{-1}$, I_{Ca}=11.7 pA, *d* = 60 nm). Data in panel *B* are the same as in Fig. 2.

Figure 5. Dependence of five-pulse FCT on the values of k_{on} and B_{total}, for a fixed value of the buffering ratio. In (*A*), κ_0 = 500; in (B), κ_0 = 50. Parameter region corresponding to SF magnitude observed at the crayfish NMJ lies inside the area bounded by contour FCT=2.0 (see text for details). Hyperbolic curves mark parameter points of constant k_{off}. In (*A*), the two curves correspond to the diagonal lines in Fig. 3 *A* and *B*. Increasing (decreasing) I_{Ca} is equivalent to sliding left (right) along these lines. Since the value of

κ_0 is fixed, K_D is determined by the value of B_{total}. Other parameters are the same as in Figs. 2-4 (D_B=0.2 $\mu m^2 ms^{-1}$, I_{Ca}=11.7 pA, d = 60 nm).

Figure 6. FCT increases with increasing distance from the Ca^{2+} channel cluster. (*A*) Five-pulse FCT as a function of B_{total} and k_{on}, at distances of *(a)* 20 nm, *(b)* 60 nm, and *(c)* 100 nm away from the edge of the channel cluster (locations marked *1* through *3* in Fig. 1). Data in panel *Ab* are the same as in Fig. 5 *A*. (*B*) $[Ca^{2+}]$ time course for parameter values corresponding to the points marked with an asterisk in *A* (B_{total}=700 μM, K_D=1.4 μM, k_{on}= 0.5 $\mu M^{-1} ms^{-1}$). Note the difference in scale along the concentration axis. Other parameter values are the same as in Figs. 2-5 (D_B=0.2 $\mu m^2 ms^{-1}$, I_{Ca}=11.7 pA).

Figure 7. Facilitation grows supralinearly in the mobile buffer case. Comparison of (*A*) simulation results with (*B*) experimental data from Fig. 3 *C* of Tang et al. (2000), showing SF for a five-pulse 100 Hz train, with and without Fura-2. In *A*, simulations are performed for parameter values corresponding to the point marked by a '*' in Fig. 6 *Ab* (distance=60 nm, B_{total}=700 μM, K_D=1.4 μM, k_{on}= 0.5 μM^{-1} ms^{-1}, D_B=0.2 $\mu m^2 ms^{-1}$, I_{Ca}=11.7 pA). Facilitation is normalized to zero for the first pulse: $([Ca^{2+}]_n / [Ca^{2+}]_1)^4 - 1$ (Eqs. 11, 12). The $[Ca^{2+}]$ trace corresponding to the control simulation curve in *A* is shown in Fig. 6 *Bb*. The following parameter values are used for the Fura-2 in *A*: B_{total}=200μM, K_D=360 nM, k_{on}= 0.27 μM^{-1} ms^{-1}, D_B=0.118 $\mu m^2 ms^{-1}$ (Tang et al., 2000).

Figure 8. Dependence of FCT on buffer mobility. Shown is the five-pulse FCT as a function of the buffer diffusion coefficient, D_B, and B_{total} (K_D), for κ_0=500. Panel *B* extends the data in panel *A* into the region of very high B_{total}, and uses logarithmic scale to emphasize the region of very small D_B. Note the two FCT peaks, one at large D_B and small B_{total}, and another peak at D_B close to zero and very large B_{total}. Parameter values: k_{on}=0.8 $\mu M^{-1} ms^{-1}$, I_{Ca}=11.7 pA, d=60 nm. The set of points along the top edge of all panels (D_B=0.2 $\mu m^2 ms^{-1}$) correspond to the horizontal line k_{on}=0.8 $\mu M^{-1} ms^{-1}$ in Figs. 5 and 6 *Ab*).

Figure 9. FCT as a function of B_{total} and k_{on} in the fixed buffer case, for a constant value of the buffering capacity, κ_0=500. Same as Fig. 6, except that D_B=0. Note that much higher B_{total} is required to achieve

significant facilitation, and the slower decay of the Ca^{2+} transients, as compared to the mobile buffer case (cf. Fig. 6).

Figure 10. Slow spatial re-equilibration of Ca^{2+} and fixed buffer after an action potential. Panels on the left (right) demonstrate the Ca^{2+} (buffer) concentration profiles respectively, at different times (indicated on the corresponding contours) after the cessation of a 1-ms-long Ca^{2+} current pulse. The profiles are shown along an axis situated 20 nm below the synaptic membrane, and running parallel to it (dot-dashed line in Fig. 2). The inset shows [Ca^{2+}] profiles on a finer concentration scale, at later times. The dashed vertical line marks the edge of the Ca^{2+} influx region (distance of 80 nm), while the long-dashed lines correspond to the three sites marked by asterisks in Fig. 1 (distances of 100 nm, 140 nm and 180 nm from the AZ center, or 20 nm, 60 nm and 100 nm from the edge of the influx region). Parameter values correspond to a point marked by a '+' in Fig. 9 *A*. At the end of the 10 ms-long interpulse interval, there is still a significant non-uniform (localized) saturation of the fixed buffer, which is in equilibrium with the locally elevated residual free Ca^{2+} (inset).

Figure 11. Facilitation grows sublinearly in the fixed buffer case. Shown is the simulated SF in response to a five-pulse 100 Hz AP train, arising from the saturation of a fixed buffer, with and without Fura-2. Note the sublinear accumulation time course, contrary to the mobile buffer case and the experimental data (cf. Fig. 7). Parameter values correspond to a point marked by a '+' in Fig. 9 *Ab*: (B_{total}=11 mM, K_D=22 μM, k_{on}= 0.2 $\mu M^{-1}ms^{-1}$; d = 60 nm). Facilitation is normalized to zero for the first pulse. Fura-2 parameters are the same as in Fig. 7 *A*. The [Ca^{2+}] trace corresponding to the control simulation curve is shown in Fig. 9 *Bb*. The residual free Ca^{2+} contributes about 12% to the fifth [Ca^{2+}] peak in the control simulation, and about 7% in the Fura-2 simulation.

Figure 12. Experimental and simulated effect of Fura-2 application on the decay time course of SF. Shown is the SF magnitude for the last pulse in a 100 Hz five-pulse train, for a variable time interval between the fourth and the fifth pulses, Δt_{4-5}, for (*A*) mobile buffer simulation, (*B*) fixed buffer simulation, and (*C*) experimental data from Fig. 3 *B* of Tang et al. (2000). SF is computed as in Fig. 7. Parameter values in (*A*) are the same as in Fig. 7 *A*, except for the faster Ca^{2+} extrusion (see text), leading to a reduction of SF at Δt_{4-5}=10 ms from 19-fold to 14-fold. Parameter values in (*B*) are the same as in Figure 11. The bi-exponential fits in (*A*) are given by 9.4 exp(-Δt/57ms) + 5.3 exp(-Δt/202ms) (*control*

simulation), and 3.7 exp(-Δt/111ms) + 3.3 exp(-Δt/ 416ms) (*simulation with Fura-2*). In (*B*), fits are 41 exp(-Δt/7.9ms) + 7.1 exp(-Δt/44ms) + 0.29 exp(-Δt/6330ms) (*control simulation*), and 21.7 exp(-Δt/7.1ms) + 1.16 (*simulation with Fura-2).*

Figure 13. Dependence of FCT on the properties of a mobile buffer, in the presence of an immobile low-affinity buffer with fixed characteristics. Five-pulse FCT is shown as a function of k_{on} and B_{total} of the mobile buffer, for mobile buffering capacity of (*A*) κ_0=500 and (*B*) κ_0=50. The buffering capacity of the immobile low-affinity buffer is κ_0^F=50, in both panels. The properties of the immobile buffer are fixed: B_{total}= 750 μM, K_D= 15 μM, k_{on}= 0.1 $\mu M^{-1}ms^{-1}$. Other parameters are the same as in Figs. 2-4 (D_B=0.2 $\mu m^2 ms^{-1}$, I_{Ca}=11.7 pA, d = 60 nm). Note that introducing an immobile low-affinity buffer reduces FCT, as compared to the single-buffer case (Fig. 5). The magnitude of this reduction is more dramatic when the capacities of the two buffers are comparable (cf. panel *B* and Fig. 5 *B*).

Model	SF site properties	SF decay mechanism	Ca^{2+} buffering requirements
1. Bound residual Ca^{2+}	Proximal, slow	Ca^{2+} unbinding from SF site	No special requirements
2. Free residual Ca^{2+} (two-site model)	Distant, fast, high-affinity	Ca^{2+} diffusion and extrusion	*Immobile*, high concentration
3a. Buffer saturation (FCT), *mobile* buffer	No specialized SF site	Ca^{2+} extrusion	*High mobility*, fast (high k_{on})
3b. Buffer saturation (FCT), *fixed* buffer		Ca^{2+} diffusion and extrusion	*Low mobility*, high capacity, high concentration

Table 1.

Symbol	Parameter name	Range of values
B_{total}	Total free buffer concentration	0 – 30 mM
k_{on}	Buffer-Ca^{2+} binding rate	0.001 – 1 $\mu M^{-1} ms^{-1}$
k_{off}	Buffer-Ca^{2+} unbinding rate	0.01 – 50 ms^{-1}
D_B	Buffer diffusion coefficient	0 – 0.2 $\mu m^2 ms^{-1}$
I_{Ca}	Calcium current per active zone	1 – 50 pA
d	Distance from the channel cluster to the SF site	20 – 100 nm

Table 2.

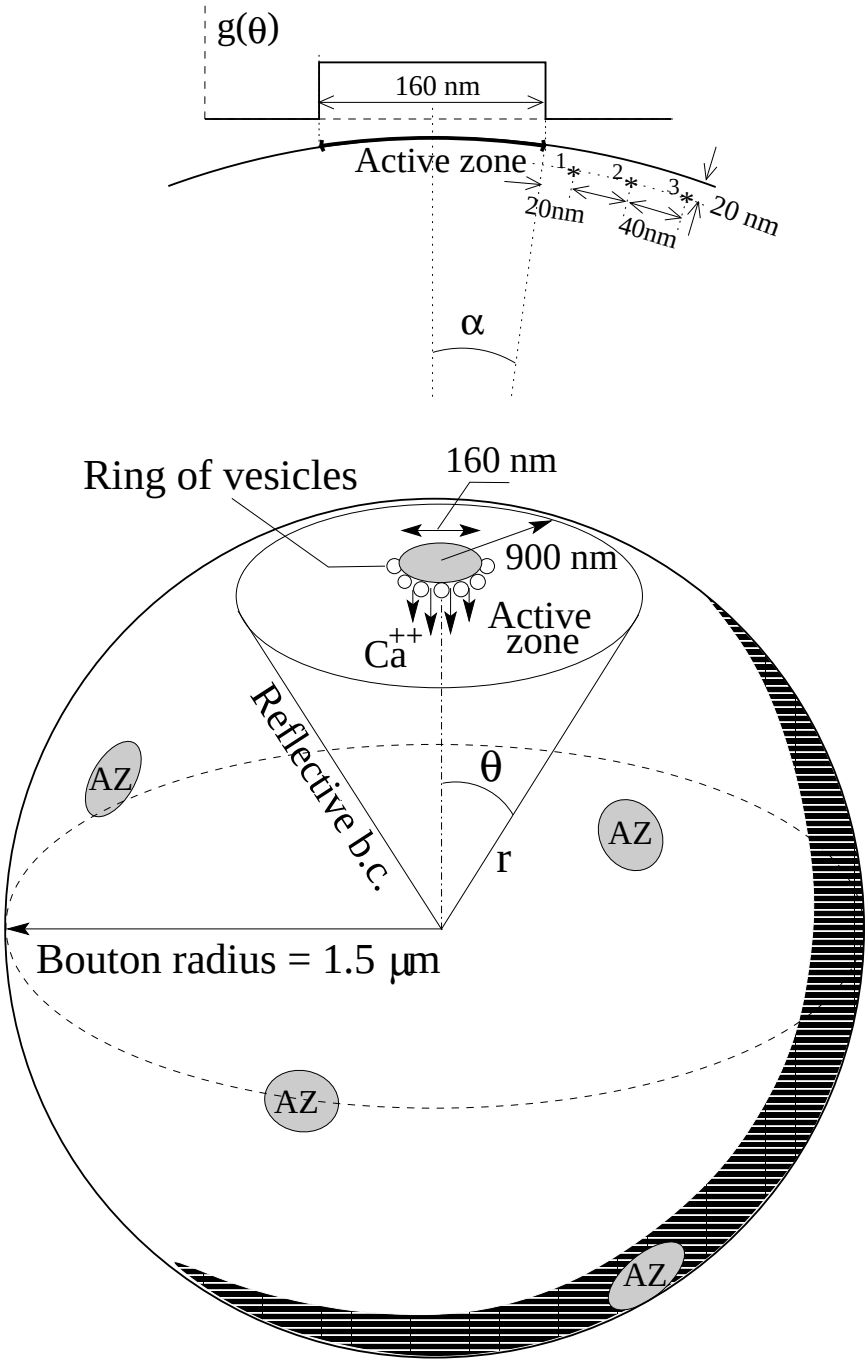
g(θ)
160 nm
Active zone
1
2
3
20nm
40nm
20 nm
α
Ring of vesicles
160 nm
900 nm
Active
zone
Ca++
Reflective b.c.
θ
r
AZ
AZ
AZ
AZ
Bouton radius = 1.5 μm

Figure 1.

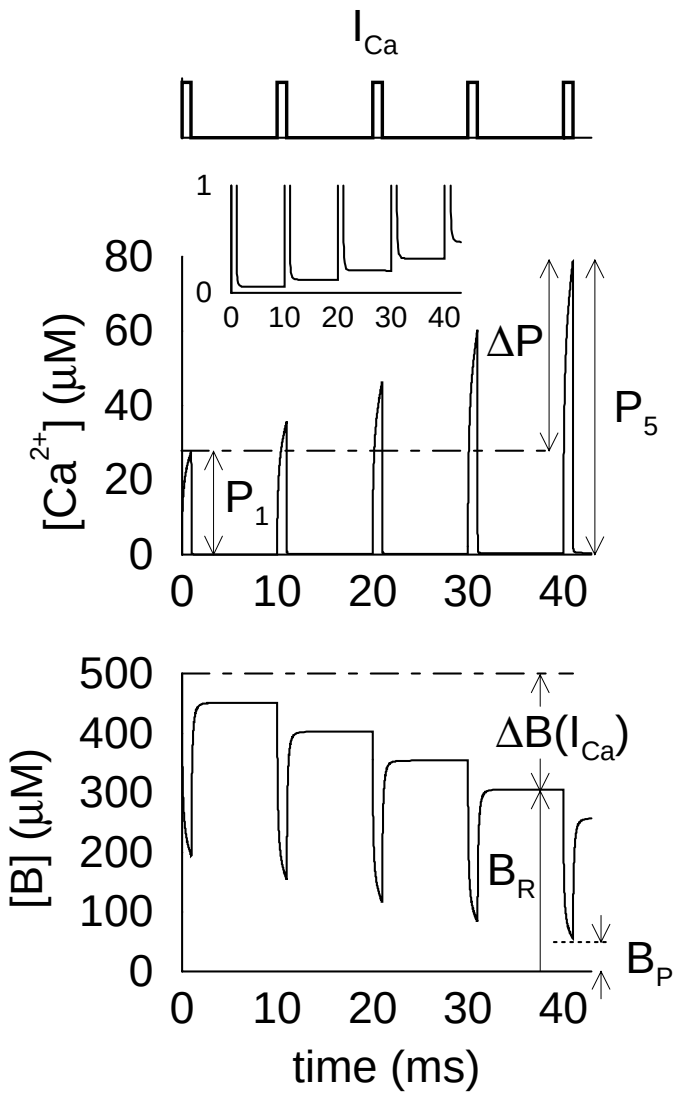
I_Ca
1
0
0 10 20 30 40
80
60
40
20
0
[Ca2+] (μM)
ΔP
P5
P1
0 10 20 30 40
500
400
300
200
100
0
[B] (μM)
ΔB(I_Ca)
B_R
B_P
0 10 20 30 40
time (ms)

Figure 2.

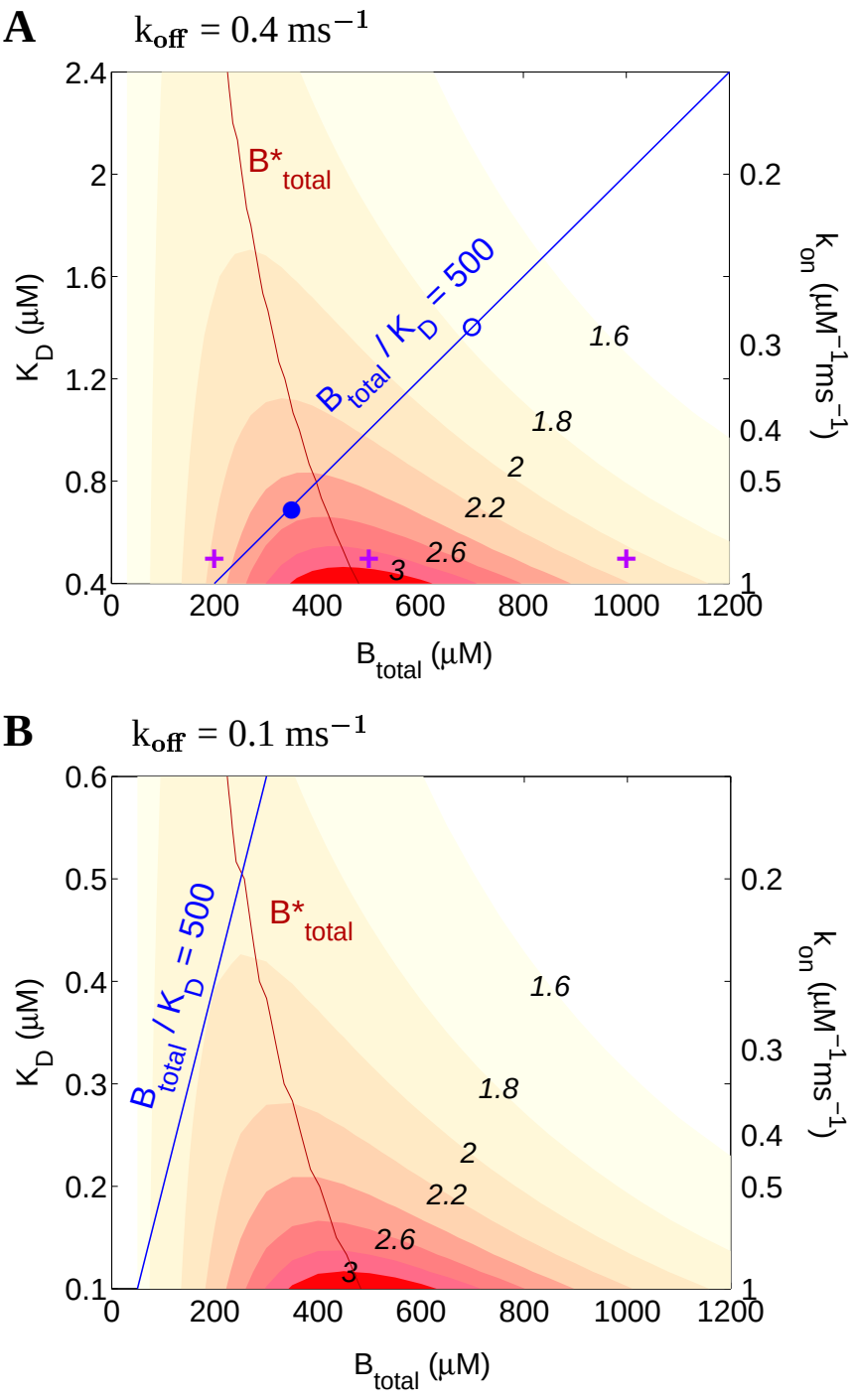
A
k_{off} = 0.4 ms^{-1}
B*total
B_{total} / K_D = 500
1.6
1.8
2
2.2
2.6
3
K_D (μM)
k_{on} ($μM^{-1}ms^{-1}$)
B_{total} (μM)
B
k_{off} = 0.1 ms^{-1}
B*total
B_{total} / K_D = 500
1.6
1.8
2
2.2
2.6
3
K_D (μM)
k_{on} ($μM^{-1}ms^{-1}$)
B_{total} (μM)

Figure 3.

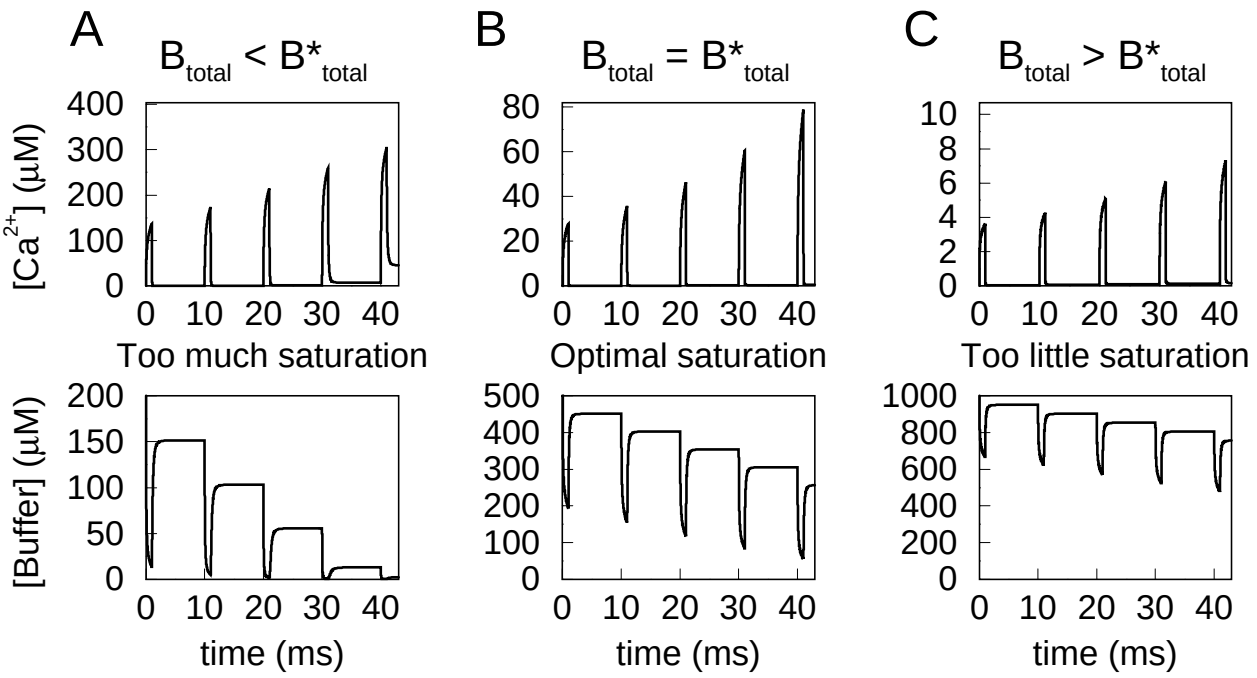
A
B
C
B_total < B*_total
B_total = B*_total
B_total > B*_total
[Ca2+] (μM)
[Buffer] (μM)
Too much saturation
Optimal saturation
Too little saturation
time (ms)
time (ms)
time (ms)

Figure 4.

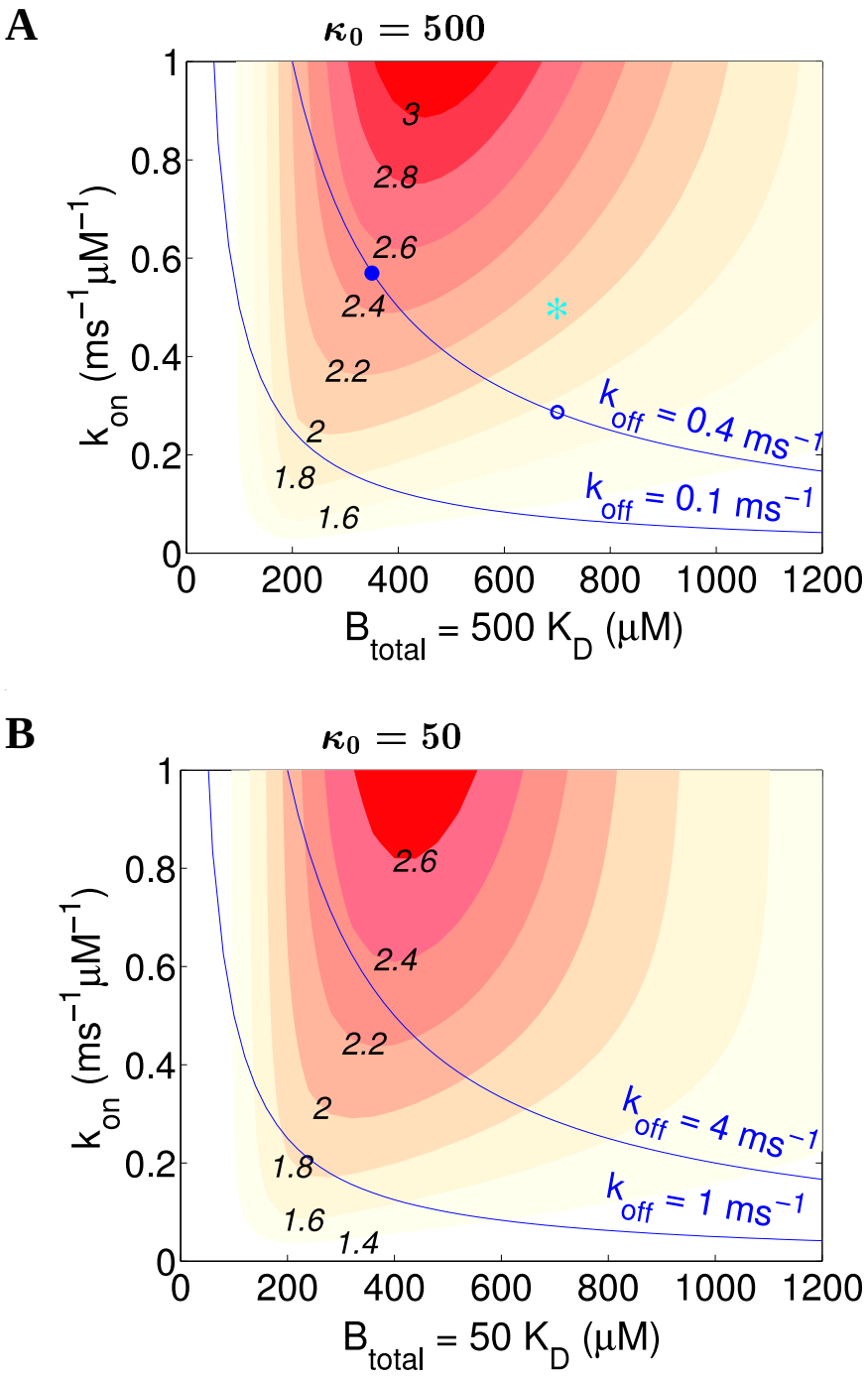
A
$\kappa_0 = 500$
3
2.8
2.6
2.4
2.2
2
1.8
1.6
k_{off} = 0.4 ms^{-1}
k_{off} = 0.1 ms^{-1}
k_{on} ($ms^{-1}\mu M^{-1}$)
B_{total} = 500 K_D (μM)
B
$\kappa_0 = 50$
2.6
2.4
2.2
2
1.8
1.6
1.4
k_{off} = 4 ms^{-1}
k_{off} = 1 ms^{-1}
k_{on} ($ms^{-1}\mu M^{-1}$)
B_{total} = 50 K_D (μM)
0
0.2
0.4
0.6
0.8
1
200
400
600
800
1000
1200

Figure 5.

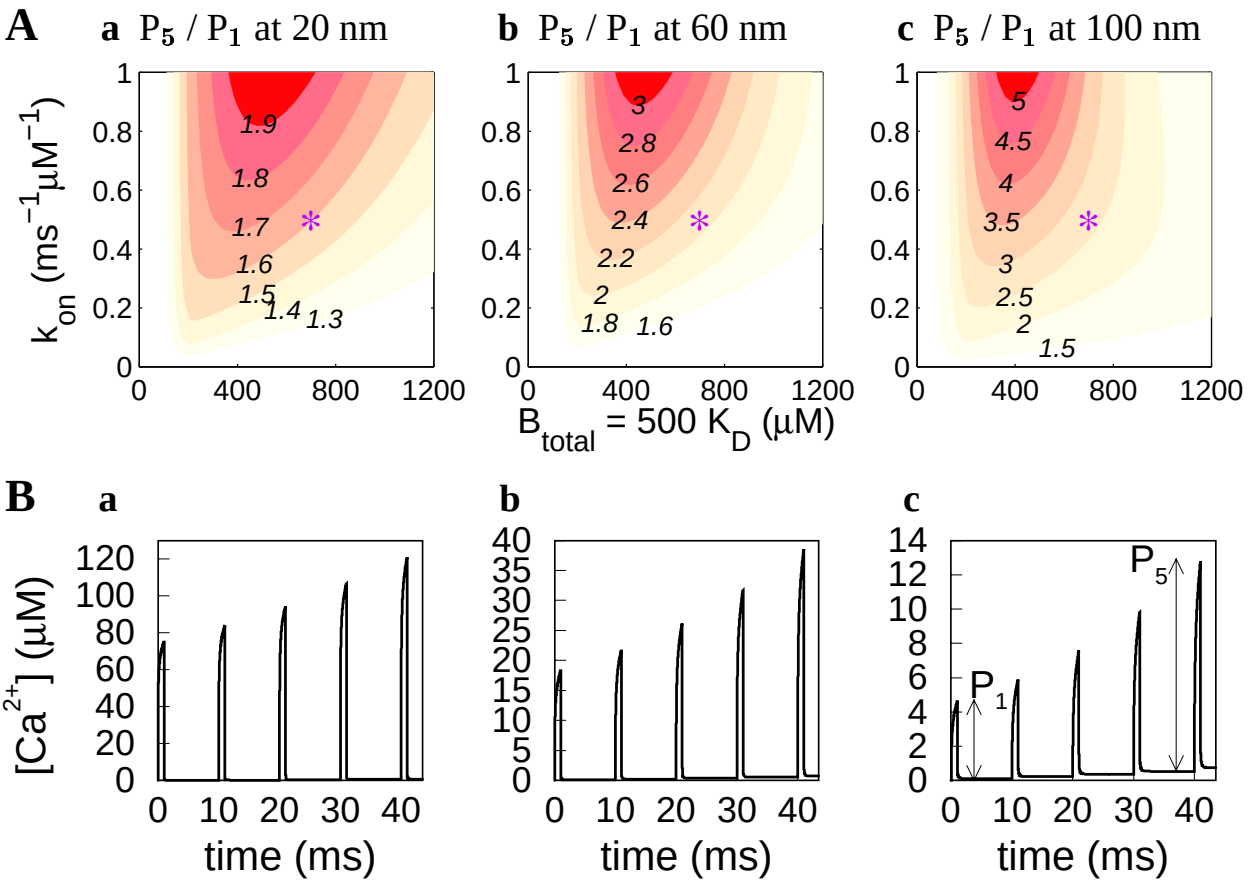
A
a P5 / P1 at 20 nm
b P5 / P1 at 60 nm
c P5 / P1 at 100 nm
kon (ms−1µM−1)
1.9
1.8
1.7
1.6
1.5
1.4
1.3
3
2.8
2.6
2.4
2.2
2
1.8
1.6
5
4.5
4
3.5
3
2.5
2
1.5
Btotal = 500 KD (µM)
B
a
b
c
[Ca2+] (µM)
time (ms)
P5
P1

Figure 6.

A

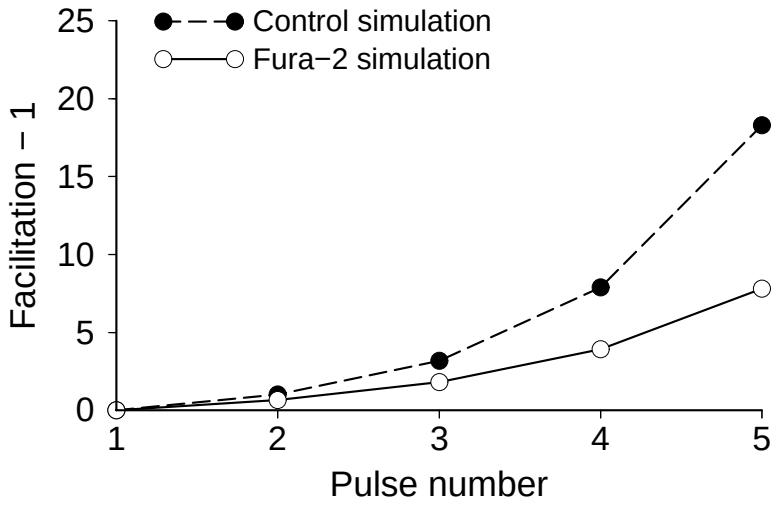
Control simulation
Fura−2 simulation
Facilitation − 1
Pulse number
0
5
10
15
20
25
1
2
3
4
5

B

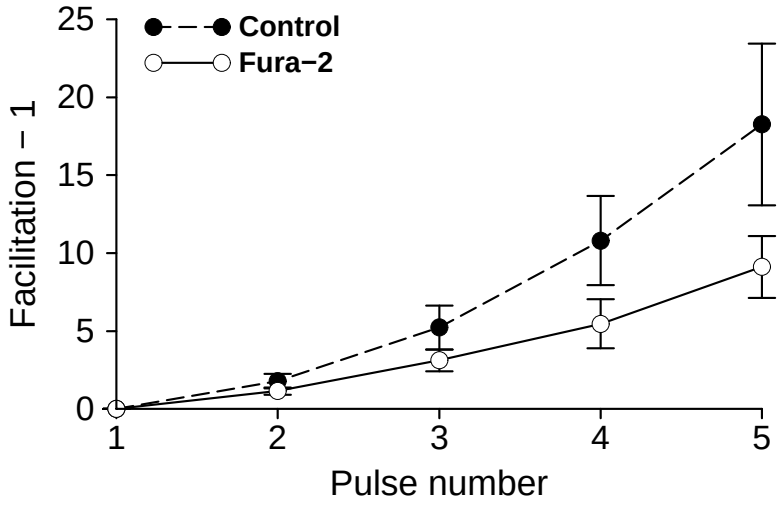
Control
Fura−2
Facilitation − 1
Pulse number
0
5
10
15
20
25
1
2
3
4
5

Figure 7.

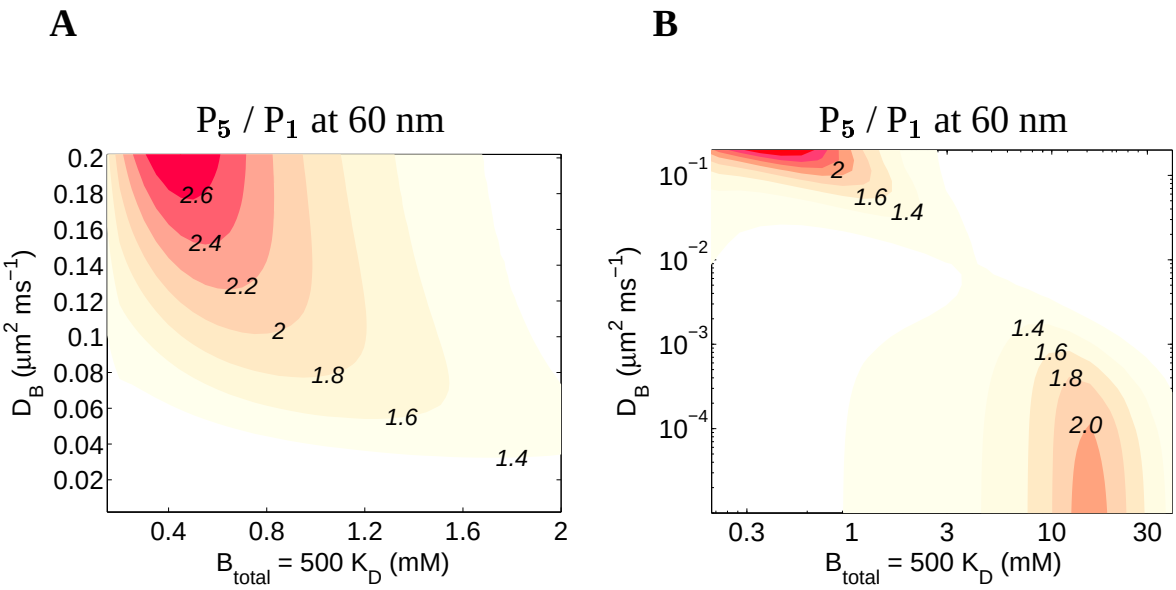
A
B
P5 / P1 at 60 nm
P5 / P1 at 60 nm
DB (μm2 ms−1)
Btotal = 500 KD (mM)
2.6
2.4
2.2
2
1.8
1.6
1.4
2.0

Figure 8.

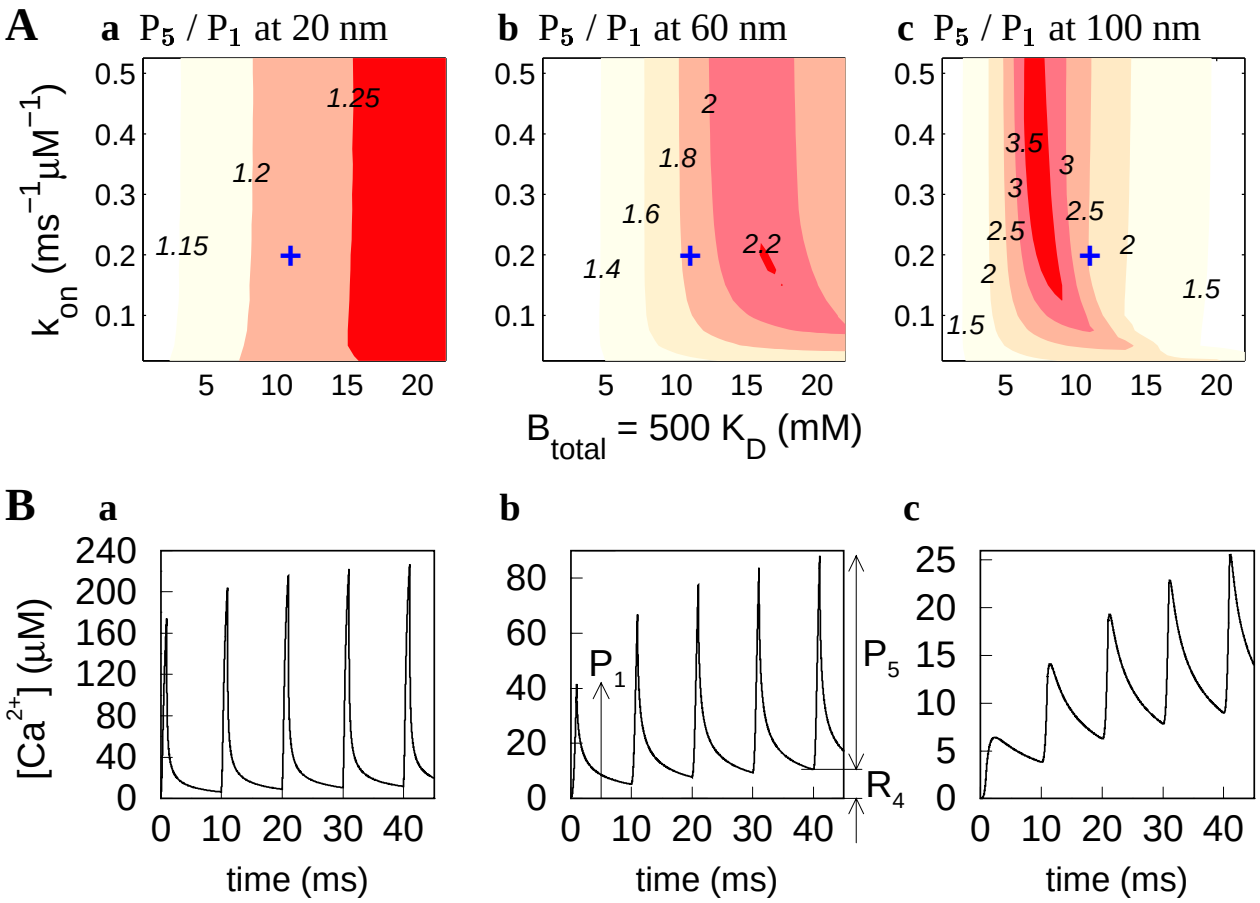
A
a P5 / P1 at 20 nm
b P5 / P1 at 60 nm
c P5 / P1 at 100 nm
kon (ms−1µM−1)
1.15
1.2
1.25
1.4
1.6
1.8
2
2.2
1.5
2
2.5
3
3.5
Btotal = 500 KD (mM)
B
a
b
c
[Ca2+] (µM)
P1
P5
R4
time (ms)

Figure 9.

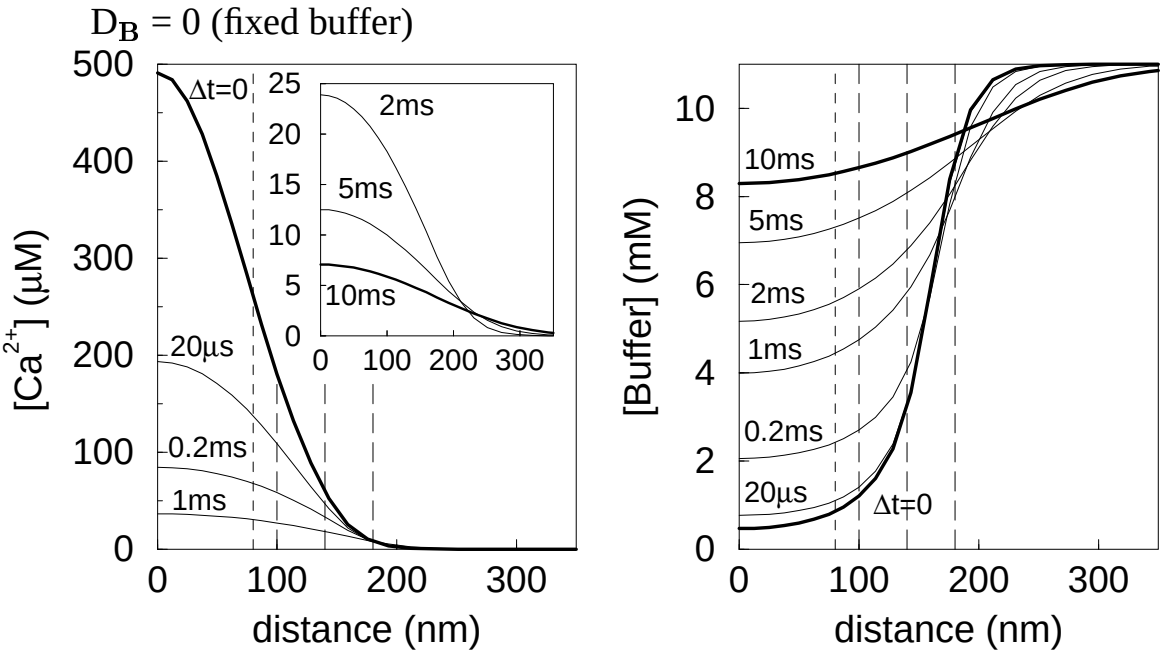
D_B = 0 (fixed buffer)
[Ca^{2+}] (μM)
distance (nm)
Δt=0
20μs
0.2ms
1ms
2ms
5ms
10ms
[Buffer] (mM)
distance (nm)
10ms
5ms
2ms
1ms
0.2ms
20μs
Δt=0

Figure 10.

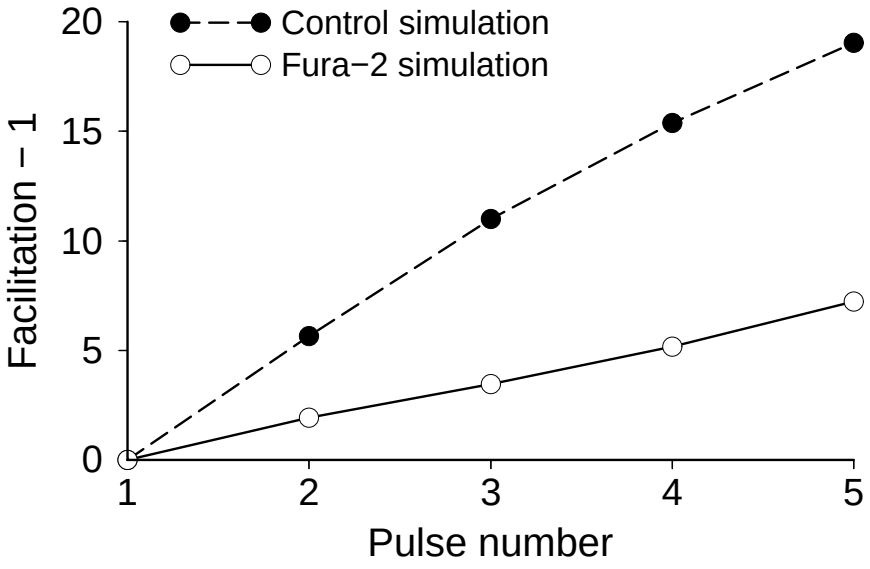
Control simulation
Fura−2 simulation
Facilitation – 1
20
15
10
5
0
1
2
3
4
5
Pulse number

Figure 11.

A

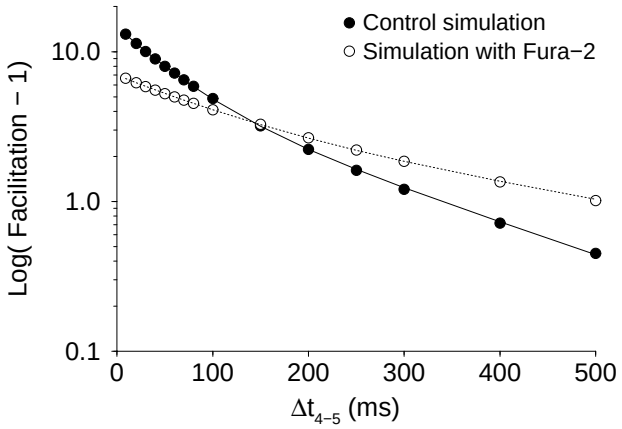

B

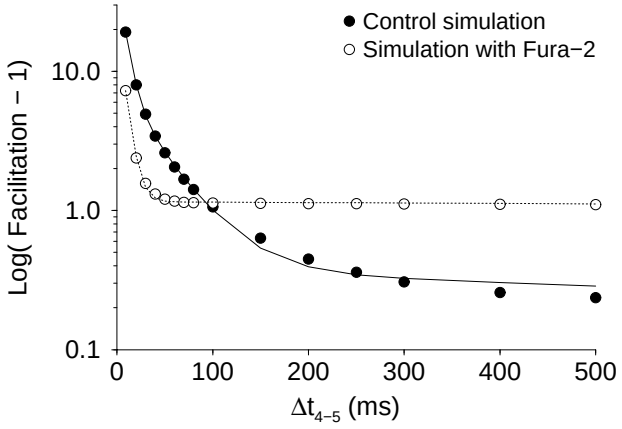

C

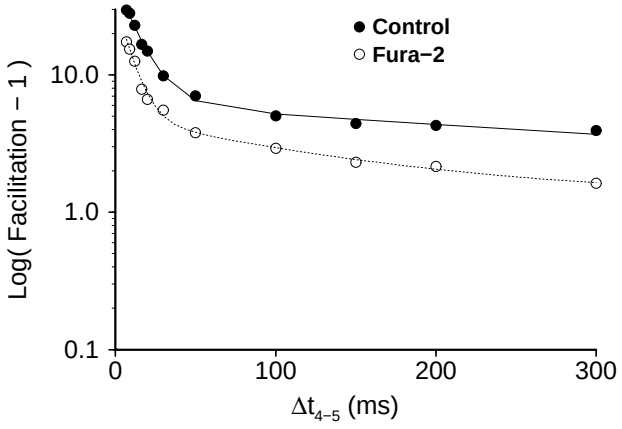

Figure 12.

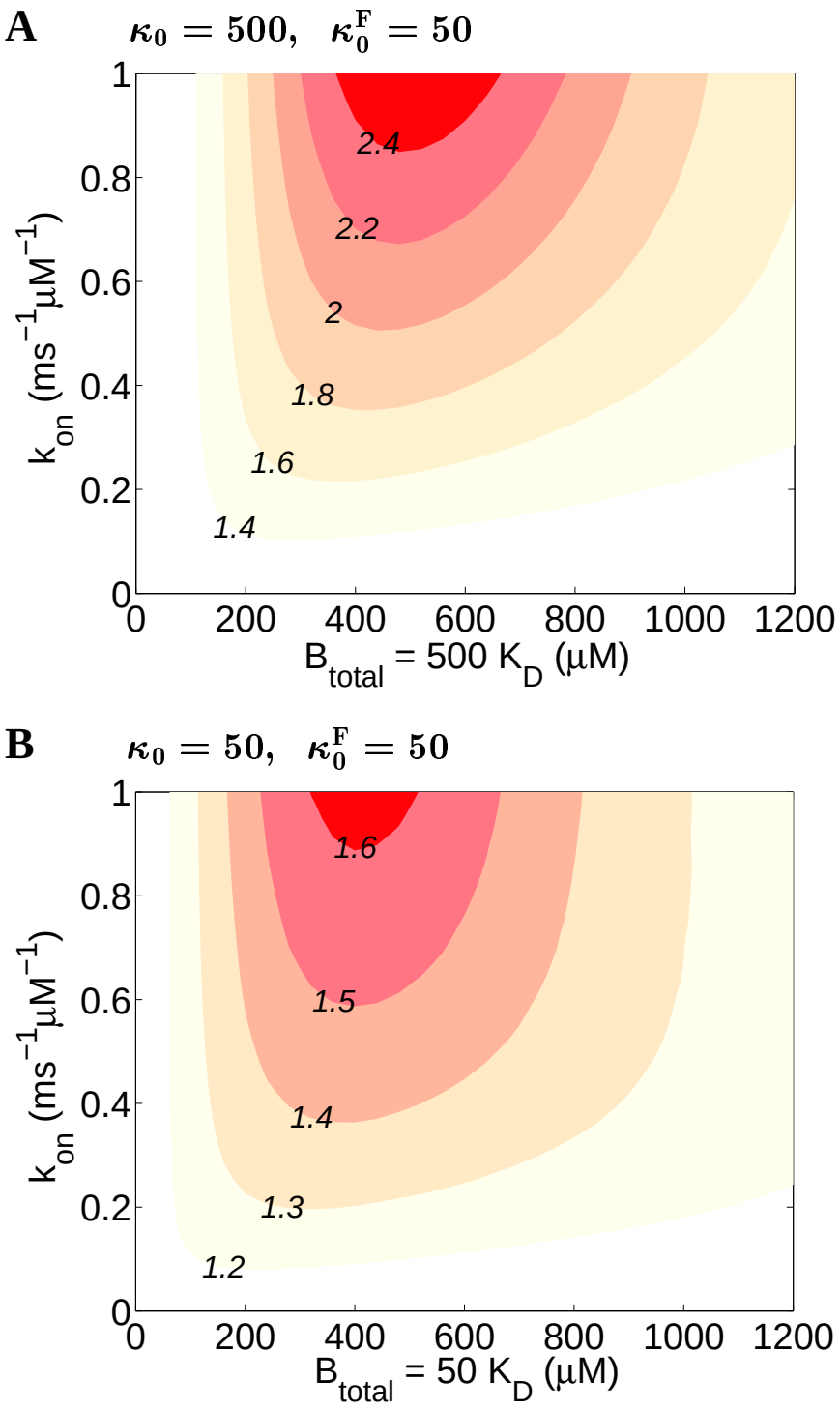
A
$\kappa_0 = 500, \quad \kappa_0^F = 50$
2.4
2.2
2
1.8
1.6
1.4
k_{on} ($ms^{-1}\mu M^{-1}$)
B_{total} = 500 K_D (μM)
B
$\kappa_0 = 50, \quad \kappa_0^F = 50$
1.6
1.5
1.4
1.3
1.2
k_{on} ($ms^{-1}\mu M^{-1}$)
B_{total} = 50 K_D (μM)

Figure 13.